Membrane Handbook

Edited by

W. S. Winston Ho, Ph.D.

and

Kamalesh K. Sirkar, Ph.D.

VNR VAN NOSTRAND REINHOLD
New York

Disclaimer

To the best of the authors' and publisher's knowledge, the information contained in this handbook is accurate. However, the publisher and authors assume no responsibility nor liability for any consequences arising from the use of the information contained herein. Final determination of the suitability of any information for use contemplated by any user is the sole responsibility of the user. In addition, the citation of commercial products, tradenames, or names of manufacturers is not to be construed as an endorsement or recommendation for use.

Library of Congress Catalog Card Number 91-43661
ISBN 0-442-23747-2

Manufactured in the United States of America

Published by Van Nostrand Reinhold
115 Fifth Avenue
New York, NY 10003

Chapman and Hall
2-6 Boundary Row
London, SE1 8HN, England

Thomas Nelson Australia
102 Dodds Street
South Melbourne 3205
Victoria, Australia

Nelson Canada
1120 Birchmount Road
Scarborough, Ontario MIK 5G4, Canada

16 15 14 13 12 11 10 9 8 7 6 5 4 3 2 1

Library of Congress Cataloging-in-Publication Data

Membrane handbook/editors, W. S. Winston Ho and Kamalesh K. Sirkar.
p. cm.
Includes index.
ISBN 0-442-23747-2
1. Membranes (Technology)—Handbooks, manuals, etc. I. Ho, W. S. Winston, 1943- , II. Sirkar, Kamalesh K., 1942-
TP159.M4M4444 1992
660'.2842—dc20

91-43661
CIP

12

Theory

Stephen B. Kessler
Sepracor Inc.

Elias Klein
University of Louisville

MASS TRANSFER: MEMBRANE

To model effectively membrane transport phenomena that pertain to dialysis, two general types of membrane models can be considered: homogeneous and porous. Homogeneous membranes are thought of as structureless continua, which, in the case of dialysis, consist of polymer-liquid gels. Porous membranes are viewed as an impervious polymer phase, interpenetrated by liquid-filled pores.

The various classes of "real" membranes described in the preceding section can be divided into the categories of homogeneous and porous, although this distinction is not always an obvious one. Since the range of pore sizes in available membranes is relatively continuous, no sharp delineation exists between homogeneous and porous. Bean (1972) has suggested a criterion for making this distinction, based on a comparison of the diffusive and hydraulic permeabilities of a given membrane.

Modeling of transport in homogeneous membranes is well matched by a phenomenological approach and a solution-diffusion theory. This theory assumes convective transport to be negligibly small. The transport properties of porous membranes can be described by continuum hydrodynamic theory, a mechanistic approach that considers the structure of the membrane. Hydrodynamic theory takes both diffusive and convective transport into account. Linear, nonequilibrium (irreversible) thermodynamics constitutes a more general phenomenological approach that can be applied to transport in either class of membrane. This approach is especially useful when multiple solutes and/or driving forces are involved.

Transport in Homogeneous Membranes: Solution-Diffusion Theory

In general, the driving force for mass transfer is a potential gradient across the membrane thickness. Phenomenological models used to describe mass transfer processes in homogeneous membranes are concerned with the relationship between this driving force and the resulting flux. In dialysis, the primary flux is that due to diffusion, which is driven by the concentration gradient component of a gradient in chemical potential. While other driving forces may exist, leading to additional fluxes (e.g., pressure gradient component of chemical potential gradient causing bulk flow), dialysis is fundamentally a diffusive process and is modeled as such by solution-diffusion theory.

The cornerstone of solution-diffusion theory, Fick's first law, is a simple phenomenological model that describes the potential/flux relationship for diffusive mass transfer in binary systems. It states that the diffusive flux is proportional to the gradient in concentration, mole fraction, or chemical potential at constant pressure. In the strictest sense, a system consisting of solute, solvent, and membrane is ternary rather than binary. However, a pseudobinary approach can be taken in which solute A diffuses through component B, where B is defined as both membrane and solvent. The molar flux of solute A can be described by the following general form of Fick's first law:

$$N_{Ay} = x_A(N_{Ay} + N_{By}) - c_t D_{AB}\frac{dx_A}{dy}, \qquad (12\text{–}1)$$

where N_{Ay} and N_{By} are the molar fluxes of A and B in the y direction, x_A is the mole fraction of solute A, c_t is the total concentration of A and B, and D_{AB} is the binary diffusion coefficient. The first term on the right represents bulk flow resulting from unequal counter diffusion of A and B, whereas the second term gives the diffusive flux.

In reasonably dilute solutions, the bulk flow term may be neglected and the total molar concentration c_t may be considered constant. Now Eq. (12–1) can be simplified to

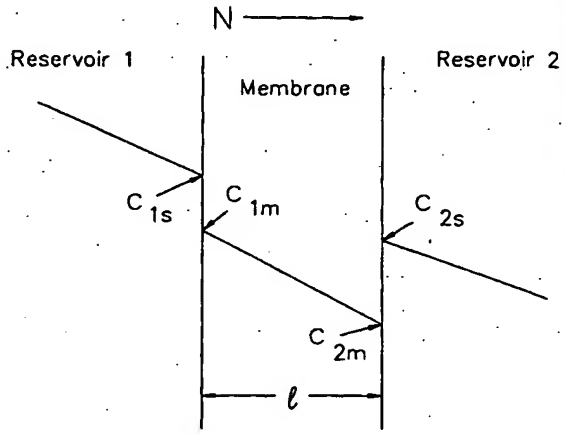

FIGURE 12–1. Typical concentration profile for diffusive transport across a membrane. In this example, the solute is less soluble in the membrane than in the external phases.

$$N_{Ay} = -D_{AB}\frac{dc_A}{dy}. \qquad (12\text{–}2)$$

Assuming a linear concentration gradient and integrating Eq. (12–2) across the membrane,

$$N_{Ay} = \frac{D_{AB}(c_{1m} - c_{2m})}{l}, \qquad (12\text{–}3)$$

where c_{1m} and c_{2m} are concentrations within the membrane at each of its interfaces and l is the membrane thickness.

Figure 12–1 shows a typical concentration profile for diffusive transport across a membrane. In this particular example, the solute is less soluble in the membrane than in either of the external solutions. Further, c_{1s} and c_{2s} are the concentrations of that solute in the external phases at the membrane/solution interfaces.

A partition coefficient K can be defined as the ratio between membrane and external solution concentrations at equilibrium:

$$K = \frac{c_{1m}}{c_{1s}} = \frac{c_{2m}}{c_{2s}}. \qquad (12\text{–}4)$$

(Note: In general $c_{1m}/c_{1s} \neq c_{2m}/c_{2s}$). Combining Eqs. (12–3) and (12–4) and simplifying by eliminating subscripts,

$$N = KD\Delta c/l. \qquad (12\text{–}5)$$

Equation (12–5) is a form of Fick's first law that is particularly well suited to membrane problems because external concentrations can be readily measured, while concentrations within the membrane, as in Eq. (12–3), cannot.

Defining a membrane diffusive permeability by

$$P_m = KD/l \tag{12–6}$$

and a membrane mass transfer resistance by

$$R_m = l/KD = l/P_m, \tag{12–7}$$

Eq. (12–5) can be written as

$$N = P_m \Delta c = \Delta c/R_m. \tag{12–8}$$

Fick's second law can be derived either from Fick's first law (Crank 1975) or the equation of continuity (Bird, Stewart, and Lightfoot 1960). It describes one-dimensional diffusion in a liquid film in which there are no chemical changes and no flow taking place:

$$\frac{dc}{dt} = \frac{D\, d^2c}{dy^2}. \tag{12–9}$$

Consider a liquid film of thickness $2l$ that contains a solute at concentration c_0. At time $t = 0$, the solute concentration at both surfaces of the film is suddenly increased to c_1. Integration of Eq. (12–9), with appropriate boundary conditions, can provide concentration profiles within the film and fluxes as a function of time.

Colton and Lowrie (1981) illustrate the solution to the unsteady-state diffusion problem posed above in the form of dimensionless concentration profiles. The dimensionless group, Dt/l^2, is the Fourier number. When $Dt/l^2 = 1$, the film is approaching a new steady-state concentration. A characteristic diffusion time, $t_D = l^2/D$, can be defined that estimates the equilibration time for diffusion across a liquid film (or a liquid-filled membrane).

Transport in Porous Membranes: Continuum Hydrodynamic Theory

Yasuda and coworkers (Yasuda, Lamaze, and Ikenberry 1968; Yasuda et al. 1969; Yasuda, Lamaze, and Peterlin 1971) developed a concept of dialytic membranes as homogeneous water-swollen gels in which thermally induced movement of segments of (coiled) polymer molecules leaves an interstitial volume free for solute transport. They concluded that the permeability characteristics of a highly swollen system cannot be described by a single coefficient. Values of solute and solvent permeabilities depend on the conditions of measurement, particularly the magnitude of convective flux relative to diffusive flux (i.e., the transmembrane Peclet number). They concluded that the following generalizations were valid:

1. The permeability of a solute, whose size is small compared to a calculated membrane pore size, is proportional to the degree of hydration of the membrane.
2. Solute permeability coefficients decrease exponentially with increasing molecular size, when the latter is expressed in terms of molecular cross-sectional area.
3. Solute rejection coefficients change markedly when the solute cross section approaches the dimension of the channels.

A different approach was used by Klein, Holland, and Eberle (1979) for a series of dialytic membranes that included not only the homogeneous, swollen gels studied by Yasuda and coworkers, but also glassy polymers having porous structures. In describing transport through either type of structure, the essence of the problem is how to describe the size distribution of the channels through which the solutes must pass, and the interactions between the solute and the channel material. The Yasuda approach was based on the statistically predictable formation and disappearance of void volumes in the hydrogel. The interaction between solute and membrane matrix material is ignored. The approach used by Klein and

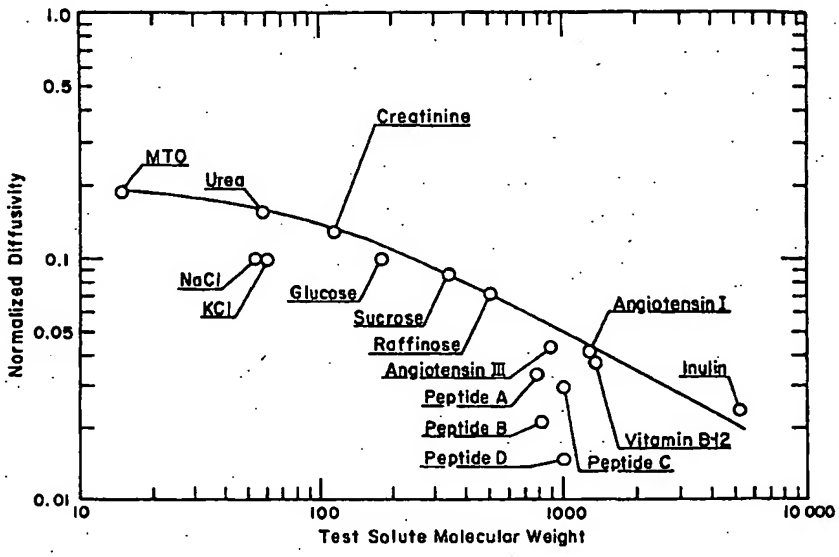

FIGURE 12–2. Plot of normalized diffusivity (D_m/D) as a function of solute molecular weight for a typical dialysis membrane (Cuprophan® 150 PM) (reprinted from Klein 1977 with permission).

coworkers based on earlier single pore channel models (Renkin 1954; Beck and Schultz 1972; Verniory et al. 1973) assumes that the membrane has a pore size distribution that can be represented by a single, hydrodynamically equivalent pore dimension. Since neither the pore fractional cross section A_p nor the actual pore length l_p can be measured independently, an experimental method is used to derive their ratio. From the Hagen-Poiseuille equation, the hydraulic permeability L_p is related to the ratio A_p/l_p and the hydrodynamic pore radius r_p by

$$L_p = \frac{A_p}{l_p}\frac{r_p^2}{8\eta}, \qquad (12\text{–}10)$$

where η is the viscosity of the solution. The value of L_p is determined by measuring the volume flux of water across the membrane in response to an applied pressure gradient. Using a diffusional model (Beck and Schultz 1972; Verniory et al. 1973), the ratio A_p/l_p can be related to the diffusive permeability coefficient P_m by

$$P_m = \frac{(A_p/l_p)D(1-q)^2}{K_1} = \frac{D_m}{l_p}, \qquad (12\text{–}11)$$

where q is the ratio of solute radius to pore radius, D is the solute diffusion coefficient in the solvent, K_1 is a power series in q, and D_m is the effective solute diffusivity in the membrane.

For a solute such as tritiated water, whose radius is small compared to the pore radius, q is approximately equal to zero, $K_1 = 1$, and the above equations can be solved simultaneously to yield

$$r_p^2 = \frac{8\eta D L_p}{P_m}. \qquad (12\text{–}12)$$

Once the single representative membrane "pore" size has been determined in this way, the permeability of any other solute of known dimensions can be calculated for the same membrane. In the absence of any specific solute/membrane interactions, such as ionic or hydrophobic bonding, this model is useful for predicting membrane permeabilities when $q < 0.6$.

On the basis of either model, dialytic transport clearly decreases as solute size increases because of two effects: Increasing molecular size implies lower solute diffusivity and increasing solute sizes produce more interfering collisions with the pore walls. The effect is seen in Figure 12–2 where the ratio of diffusivity in the membrane D_m to the solution diffusivity D (defined as normalized diffusivity) is plotted as a function of solute molecular weight. At the low molecular weight end of the plot, the impedance of the membrane reduces diffusivity to 50 to 80% of the free solution diffusivity. Membrane impedance can be defined quantitatively

as (1 – normalized diffusivity). At higher molecular weights—where solute sizes approach the dimensions of the membrane channels—the impedance is more than 99%.

Irreversible Thermodynamics

The simultaneous presence of both concentration and pressure driving forces results in a mixed diffusive-convective transport process. When both diffusive and convective fluxes are of significant magnitudes, both must be accounted for, as well as their interactions. Irreversible thermodynamics provides a framework for analyzing these complex interactions between fluxes and forces. Irreversible thermodynamics has been applied to membranes by Kedem and Katchalsky (1958) and Katchalsky and Kedem (1962) based on the fundamental work of Onsager (1931a, 1931b). In addition to the reviews by Katchalsky and Curran (1965) and Bean (1972), this topic has been discussed from a membrane perspective by Bungay (1986) and Spriggs and Li (1976).

The hydraulic permeability of a membrane, L_p, is expressed in the form of a coefficient of proportionality between volumetric flux (superficial velocity) J_v and transmembrane pressure difference Δp as shown in Eq. (12–13):

$$J_v = L_p \Delta p \qquad (\Delta \pi_s = 0). \tag{12–13}$$

Equation (12–13) applies in the absence of an osmotic pressure difference ($\Delta \pi_s = 0$). If this is not the case, then osmotic pressure differences across the membrane will affect the flux. This situation is described by Eq. (12–14):

$$J_v = L_p \Delta p + L_{pD} \Delta \pi_s, \tag{12–14}$$

where L_{pD} is the coefficient of osmotic flow. A second phenomenological equation defines the differential rate of transport of solute and solvent, J_D:

$$J_D = L_{Dp} \Delta p + L_D \Delta \pi_s, \tag{12–15}$$

where L_{Dp} is defined as the ultrafiltration coefficient and L_D is the diffusional mobility per unit osmotic pressure difference.

By Onsager's law, $L_{pD} = L_{Dp}$. Thus, three measurements are required to characterize a given membrane-solvent-solute system. One experiment is suggested by Eq. (12–13): measurement of hydraulic permeability L_p in the absence of an osmotic pressure difference.

In the case of a selective membrane with solute present, a difference in solute and solvent fluxes is observed. This exchange flow is described by Eq. (12–16), and it provides a means of measuring L_{Dp}:

$$J_D = L_{Dp} \Delta p \qquad (\Delta \pi_s = 0). \tag{12–16}$$

A third experiment can be done with no hydrostatic pressure difference, but with solute concentration differing across the membrane ($\Delta \pi_s > 0$). In this case, both an exchange flow and an osmotic flow take place. The exchange flow defines L_D and is described by Eq. (12–17):

$$J_D = L_D \Delta \pi_s \qquad (\Delta p = 0). \tag{12–17}$$

A useful transformation of Eqs. (12–14) and (12–15) is given below. Staverman (1951) defined a reflection coefficient σ:

$$\sigma = -(L_{pD}/L_p). \tag{12–18}$$

At zero volume flow, the solute flux J_s can be related to the osmotic pressure by a solute permeability coefficient ω:

$$\omega = J_s/\Delta \pi_s \qquad (J_v = 0), \tag{12–19a}$$

where ω is related to the membrane permeability P_m through the van't Hoff equation. Thus,

$$P_m = \omega RT. \tag{12–19b}$$

With the coefficients defined by Eqs. (12–18), (12–19a), and (12–19b), the transformed phenomenological equations are (Kedem and Katchalsky 1958; Katchalsky and Curran 1965):

$$J_v = L_p \Delta p - \sigma L_p \Delta \pi_s, \tag{12–20}$$

$$J_s = c_s(1 - \sigma)J_v + \omega\Delta\pi_s. \quad (12\text{–}21)$$

Equations (12–20) and (12–21) are known as the Kedem-Katchalsky equations.

For systems involving multiple solutes, coupling occurs in the sense that the chemical potential gradient of each solute affects the flux of all solutes. Fick's laws, being limited to binary systems, do not account for coupling. The nonequilibrium thermodynamics approach considers that all fluxes depend on all forces, thus providing an appropriate theoretical framework within which to account for coupling.

Nonideal Effects

The plot of reduced diffusivities as a function of molecular weight can be misleading when applications are projected from such data. On the basis of the reduced diffusivity for the examples shown, almost no transfer of solutes greater than about 5000 dalton would be expected. However, in "real-world" devices mass transfer occurs in the presence of differential transmembrane pressures. The need to flow feed and dialysate solutions past the membrane surfaces creates obligatory pressure drops in the respective channels. When these are unequal, transfer occurs by convective modes as well as by dialytic transfer. Moreover, the presence of nonpermeating species may create osmotic pressures that oppose the applied hydraulic pressure differences. Thus, the computation of mass transfer in a device is often quite a bit more complicated than in a laboratory test cell in which flow and pressure conditions can be controlled more closely.

But even under the more or less ideal circumstances of laboratory test cells, nonideal effects stem from interactions between the feed solution and the membrane. For membranes made from hydrophobic polymers, the best described phenomenon is solute adsorption within the pores. Strong hydrophobic bonding between large solutes, such as peptides and proteins, can alter the effective pore dimensions of the dialysis membranes. This is reflected in reductions of both the hydraulic permeability and the dialytic transfer of large solutes.

MASS TRANSFER: OVERALL

In an overall sense, mass transfer in the dialysis process involves three phases: feed, membrane, and dialysate. In addition to the resistance to solute diffusion encountered in the membrane, diffusional resistances in each of the two liquid phases result in concentration gradients adjacent to the membrane. Within these boundary layers, solute concentration differs from that of the bulk solution. The magnitude of the mass transfer resistance across such a boundary layer is dependent on the thickness of the layer, which depends, in turn, on fluid flow parameters. Mass transfer coefficients are a convenient means of quantifying mass transfer rates in the case of the two moving fluid phases, feed and dialysate, for both laminar and turbulent flow. As shown in Eq. (12–22), the mass transfer coefficient k is defined by an expression of the same form as Fick's first law [see Eqs. (12–5) and (12–8)]. The concentration difference Δc is that between the membrane surface and the bulk liquid:

$$N = k\Delta c, \quad (12\text{–}22)$$

where k replaces the permeability P_m, which in Fick's first law is based on a constant film thickness. Mass transfer coefficient k is expressed in the same units as P_m, that is, linear velocity, and, like P_m, is the reciprocal of mass transfer resistance, but unlike P_m, is based on a variable film thickness. The combined effects of simultaneous convective and diffusive mass transfer that occur in permeable ducts are difficult to analyze theoretically. Mass transfer coefficients are useful, both as a means of expressing analytical results and as a measurable experimental parameter in cases for which analysis is inadequate.

Consider a dialyzer of unspecified geometry operating countercurrently. The feedside flow is assumed to be laminar, while the dialysate flow is assumed to be turbulent. The velocity profiles for this case are illustrated by Keller (1973), as shown in Figure 12–3(a). Solutes in the feed are convected parallel to the membrane surface, diffuse through the membrane phase, and are then transferred by convection again in

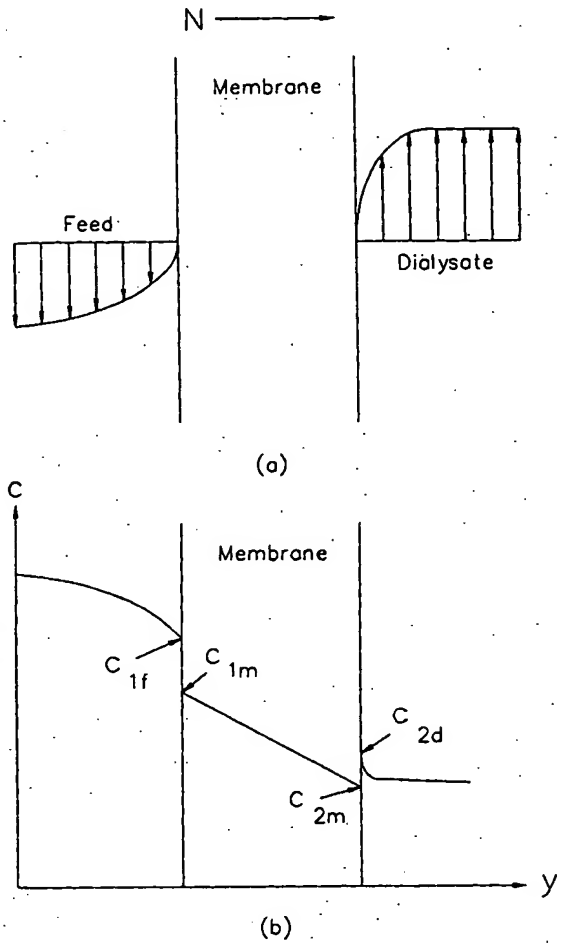

FIGURE 12–3. (a) Velocity profiles for the case of laminar feed flow and turbulent dialysate flow. (b) Concentration profiles corresponding to the velocity profiles in (a) (after Keller 1973).

the dialysate. Figure 12–3(b) shows the resulting (qualitative) concentration profiles at a single point with respect to the length of the dialyzer.

The overall mass transfer resistance R_o can be expressed as the sum of the resistances associated with each phase:

$$R_o = R_f + R_m + R_d, \qquad (12\text{–}23)$$

where the subscripts f, m, and d refer to feed, membrane, and dialysate, respectively.

The overall mass transfer coefficient k_o is the reciprocal of R_o:

$$k_o = 1/R_o. \qquad (12\text{–}24)$$

Thus,

$$1/k_o = 1/k_f + 1/P_m + 1/k_d. \qquad (12\text{–}25)$$

Considering now the length coordinate, both momentum and concentration boundary layers develop along the length of a flow conduit as shown in Figure 12–4. Most practical devices operate such that the momentum boundary layer is fully developed within a negligibly short axial distance, while, in the same devices, concentration boundary layers develop throughout their length. As a result, the local mass transfer coefficient, as defined above, varies throughout the length of the device and is difficult to measure experimentally. A length-averaged, overall mass transfer coefficient is a readily measured parameter. It expresses the relationship between the average molar flux N and a length-averaged concentration difference $\overline{\Delta c}$:

$$N = \bar{k}_o \overline{\Delta c}. \qquad (12\text{–}26)$$

Evaluating $\bar{k}_o$ can be done analytically for laminar flow in tubes and rectangular ducts. For irregular geometries and/or turbulent flows, empirical correlations can be used. In either case, the heat transfer literature serves as a basis, and dimensionless groups provide an efficient means of expressing the results.

Mass Transfer in Permeable Ducts with Laminar Flow

In some dialyzer designs, in particular, hemodialyzers for which extracorporeal blood volume must be minimized, the feedside flow is channeled through relatively thin ducts and is laminar in nature. As stated above, this situation lends itself to an analytical approach.

The Sherwood number (analogous to the Nusselt number in heat transfer) is a form of dimensionless mass transfer coefficient. It is defined by

$$\mathrm{Sh} = kL/D, \qquad (12\text{–}27)$$

where L is a length characteristic of the duct geometry and D is the diffusion coefficient of the solute species under consideration.

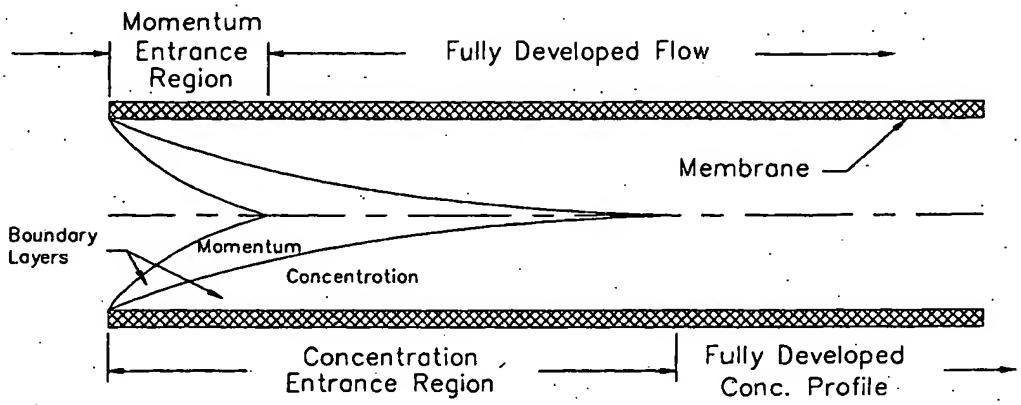

FIGURE 12–4. Flow conduit within a diffusive mass transfer device showing development of momentum and concentration boundary layers (after Colton and Lowrie 1981).

A length-averaged, feedside Sherwood number $\overline{\mathrm{Sh}}_f$ can be defined as

$$\overline{\mathrm{Sh}}_f = \bar{k}_f L/D. \tag{12–28}$$

This $\overline{\mathrm{Sh}}_f$ can be related to experimentally measurable concentrations as well as estimated analytically for laminar flow in regularly shaped ducts. Equations (12–29) and (12–30) define a dimensionless concentration c^* and a dimensionless axial length z^* for laminar flow in a porous tube:

$$c^* = (c_b - c_f)/(c_d - c_f), \tag{12–29}$$

$$z^* = zD/vd_{ti}^2, \tag{12–30}$$

where c_b is the average bulk solute concentration in the feed duct, c_f and c_d are solute concentrations in the feed (as it enters) and dialysate, respectively, z is distance in the axial direction, D is the solute diffusion coefficient, v is average axial velocity, and d_{ti} is the diameter of the tube.

Equation (12–31) defines a wall Sherwood number (Sh_w), the ratio of the concentration gradient in the fluid adjacent to the wall to that in the wall, and Eq. (12–32) defines a length-averaged overall Sherwood number ($\overline{\mathrm{Sh}}_o$) in terms of the previously defined feedside and wall Sherwood numbers:

$$\mathrm{Sh}_w = k_w d_{ti}/D, \tag{12–31}$$

$$1/\overline{\mathrm{Sh}}_o = 1/\mathrm{Sh}_w + 1/\overline{\mathrm{Sh}}_f. \tag{12–32}$$

Solution of the convection-diffusion equation with appropriate boundary conditions gives values for Sh_o, from which values for $\overline{\mathrm{Sh}}_f$ may be calculated using Eq. (12–32). Colton and coworkers (Colton and Lowrie 1981; Colton 1969; Colton et al. 1971) have reviewed various solutions for tubes and rectangular ducts. The classical Graetz problem is stated for laminar flow heat transfer in a tube with constant temperature at the wall, analogous to constant wall concentration in the mass transfer problem. Lévêque's solution (Lévêque 1928) assumes a linear velocity profile near the wall and is valid in the concentration entrance region. This solution is a useful approximation in many cases and is given in Eq. (12–33):

$$\overline{\mathrm{Sh}}_f = 1.62z^{*-0.33}. \tag{12–33}$$

Colton (1969) solved the case of a constant flux boundary condition with finite wall permeability for rectangular channels, which is more pertinent to a typical dialysis process. Davis and Parkinson (1970) solved the equivalent case for tubes. These solutions are shown graphically by Colton and Lowrie (1981) and Colton (1988). Their graph of the Davis and Parkinson solution for tubes is reproduced in

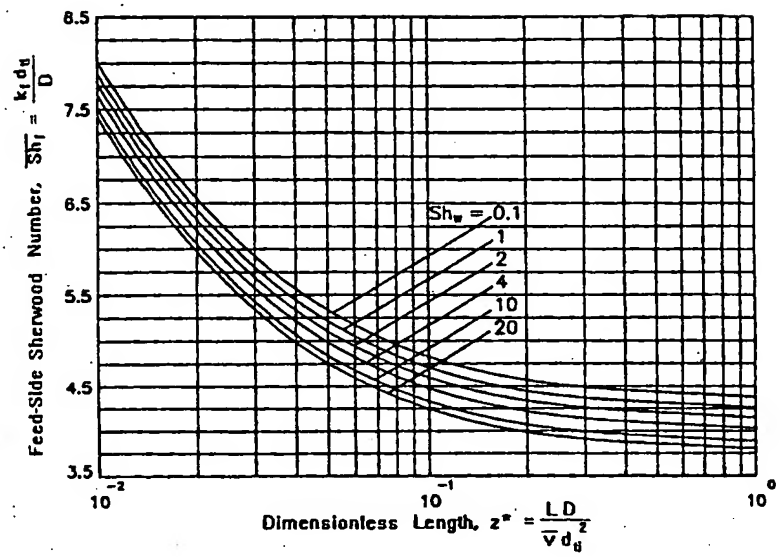

FIGURE 12–5. Davis and Parkinson solution for laminar-flow mass transfer in a tube with permeable walls—constant flux boundary condition. The family of curves represents values of the wall Sherwood number Sh_w (after Colton and Lowrie 1981).

Figure 12–5, which shows a family of curves covering a range of wall Sherwood numbers from $Sh_w = 0.1$ to 20. In the concentration entrance region (dimensionless length $z^* < 10^{-2}$), the Lévêque solution is a good approximation to the Davis and Parkinson solution. At higher values of dimensionless length, corresponding to more fully developed boundary layers, the Lévêque solution tends to underpredict the Sherwood number and does not predict the asymptotic value of $\cong 4$ predicted by both Davis and Parkinson for tubes and Colton for rectangular channels.

Subsequently, Cooney, Davis, and Kim (1974) and Jagannathan and Shettigar (1977) included a variable dialysate-side resistance in reformulating the analysis as a conjugated boundary value problem for parallel-plate and hollow-fiber configurations, respectively. These latter approaches require solution by numerical methods. The analysis of Jagannathan and Shettigar for hollow fibers, which also considers the effects of ultrafiltration, predicts that, for constant membrane area, fiber diameter and length have very little effect on overall mass transfer for low-permeability membranes. However, for high-permeability membranes, overall mass transfer decreases with increasing membrane diameter.

Mass Transfer in Irregular Geometries with or without Turbulent Flow

The dialysate-side flow in many dialyzer designs occurs within an irregular geometry and may be turbulent as well. Analysis of these situations is difficult and the resulting predictions tend to exhibit larger errors than in the above case of laminar flow in well-defined ducts. Instead, correlations from empirical heat and mass transfer studies are usually employed.

One dialysate-side flow configuration that has been treated analytically is the shell side of hollow-fiber dialysis modules. The starting point for these analyses is modeling of laminar flow relative to arrays of cylinders. (Most hollow-fiber dialyzers contain sufficiently small diameter fibers at high enough packing densities that shellside flow is laminar). The "free surface" or "equivalent annulus" model of Happel (1959) applies to flow either parallel or perpendicular to the cylinder's axes and is limited to low packing densities. Sparrow and Loeffler (1959) obtained an analytical solution for the parallel flow case that applies at high as well as at low packing densities, where it agrees with Happel's model.

Hermans (1978), Noda and Gryte (1979), and Gostoli and Gatta (1980) have developed

models for hollow-fiber dialyzer performance that incorporate dialysate-side mass transfer resistance. Hermans makes use of an equivalent annulus approximation to model a hollow-fiber dialyzer with shellside flow perpendicular to the fibers. Gostoli and Gatta apply the same approximation to parallel flow in both cocurrent and countercurrent directions. They define a parameter, α, which is the ratio of the inside diameter of the fictitious annulus to the fiber outside diameter. Fiber packing density Φ can be defined by

$$\Phi = Nd_{to}^2/d_S^2, \qquad (12\text{–}34)$$

where N is the number of fibers, d_{to} is the fiber outside diameter, and d_S is the inside diameter of the module shell. The quantity α can also be defined as the square root of Φ. For values of $\alpha < 0.635$ ($\Phi < 0.4$), estimation of Sherwood numbers by the equivalent annulus approximation is accurate to within 5% (Gostoli and Gatta 1980).

Noda and Gryte (1979) applied the complete Sparrow-Loeffler solution to dialysate-side mass transfer without the usual simplifying assumptions. Their model takes into account the interactions between neighboring fibers that occur at higher packing densities. Figure 12–6 shows the values predicted for the various Sherwood numbers by their model. Maxima for both dialysate-side Sherwood number, $\overline{Sh}_d$, and overall Sherwood number, $\overline{Sh}_o$, are predicted to occur at a packing density value of 0.63. Analyses based on the equivalent annulus approximation (Hermans 1978; Gostoli and Gatta 1980) neglect interactions between fibers and predict Sh_o to increase with packing density without reaching a maximum.

All of the above authors assume regular arrays of cylinders, either triangular or square, in their analyses. The authors of the hollow-fiber models (Hermans 1978; Noda and Gryte 1979; Gostoli and Gatta 1980) all recognize that real dialyzers represent randomly distributed arrays whose behavior can deviate significantly from that of ideally distributed models. One form of deviation that can occur is channeling

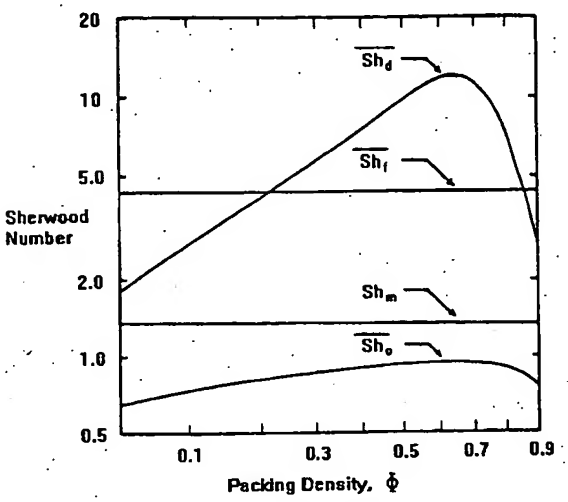

FIGURE 12–6. Sparrow-Loeffler solution for axial-flow shellside mass transfer, including interactions between fibers. Assuming a regular, triangular array, the model predicts maxima in both dialysate-side and overall Sherwood numbers ($\overline{Sh}_d$ and $\overline{Sh}_o$) at a packing density of $\Phi = 0.63$ (after Noda and Gryte 1979).

or maldistribution of flow, which is discussed further in Chapter 13. In general, these deviations compromise the efficiency of real dialyzers and the model predictions should be viewed as an upper limit of achievable performance.

Devices that deviate significantly from model predictions can be treated with correlations obtained empirically for similar devices. This approach can be used in both laminar and turbulent flow and for virtually any geometry. In this type of correlation, the Sherwood number is usually defined in terms of other dimensionless groups whose values can be measured experimentally. The Reynolds number, Re, characterizes fluid flow as a ratio of inertial-to-viscous forces, while the Schmidt number, Sc, expresses the relationship between momentum diffusivity and molecular diffusivity:

$$\mathrm{Re} = \rho v L/\eta, \qquad (12\text{–}35)$$

$$\mathrm{Sc} = \eta/\rho D, \qquad (12\text{–}36)$$

where ρ is the fluid density, v is a characteristic velocity, L is a characteristic length, η is the

fluid viscosity, and D is the solute diffusion coefficient.

The general expression for local Sherwood number is given by

$$\text{Sh} = f(\text{Re, Sc, duct geometry}). \quad (12\text{–}37)$$

For a length-averaged Sherwood number, the dependency on duct geometry drops out and correlations of the form of Eq. (12–38) are used:

$$\text{Sh} = a(\text{Re}^b, \text{Sc}^c), \quad (12\text{–}38)$$

where a, b, and c are empirically determined constants.

Spriggs and Li (1976), Yang and Cussler (1986), Klein, Ward, and Lacey (1987), and Prasad and Sirkar (1988) have reviewed mass transfer correlations published for heat and mass transfer studies for flow external to tubes. Values reported in the literature for constant b vary from 0.33 to 0.93. The lower end of this range probably results from flows that are laminar in nature, while the upper end may reflect effects such as movement of flexible tubes (e.g., hollow fibers) in response to the external flow field. A value of 0.67 (⅔) is generally accepted for turbulent flow. Better agreement is seen for the value of c, which ranged from 0.32 to 0.38 and is usually fixed at 0.33 (⅓). Constant a varies considerably and appears to depend on the geometry of the system.

If a given system is similar in its geometry and fluid flow to one for which an established correlation exists, then applying the published values for the constants a, b, and c will probably predict its performance with reasonable accuracy. If this is not the case, then a Wilson plot may be used to correlate data from the new system. In this procedure, first used by Wilson (1915) to analyze heat transfer resistances, the relationship between dialysate mass transfer coefficient $\bar{k}_d$ and dialysate flow is assumed to follow a relationship defined by

$$\bar{k}_d = AQ_d^b, \quad (12\text{–}39)$$

where Q_d is the dialysate flow rate and A and b are constants specific to the flow geometry and solute under study. Then, substituting in Eq. (12–25) gives

$$1/\bar{k}_o = 1/\bar{k}_f + 1/P_m + 1/AQ_d^b. \quad (12\text{–}40)$$

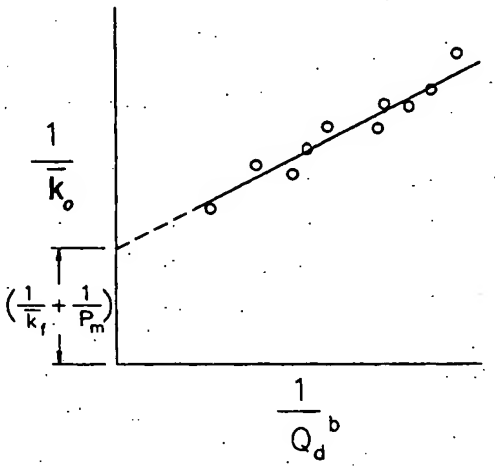

FIGURE 12–7. Wilson plot used to correlate shellside mass transfer data from devices for which a specific correlation has not been established.

The quantity $\bar{k}_o$ is measured at several values of Q_d and $1/\bar{k}_o$ is plotted versus $1/Q_d^b$ as shown in Figure 12–7. A value for b is chosen that gives the best straight-line fit to the data. The intercept of this line corresponds to infinite dialysate flow rate at which $1/\bar{k}_d$ is zero. Thus, the value of the intercept equals $(1/\bar{k}_f + 1/P_m)$ and $1/\bar{k}_d$ at any Q_d can be determined by subtracting the intercept from the corresponding value of $1/\bar{k}_o$.

Dialysis-Specific Mass Transfer Parameters

In the previous section, mass transfer was discussed for the liquid phases adjacent to the membrane. For practical applications, this analysis must be extended to describe mass transfer for the dialyzer as a whole. Neglecting convective contributions, we can write the following equation for the moles of solute, dQ_i, transferred across an element of membrane of length dz and area dA_m per unit time (Figure 12–8):

$$dQ_i = k_o(c_f - c_d)\, dA_m, \quad (12\text{–}41)$$

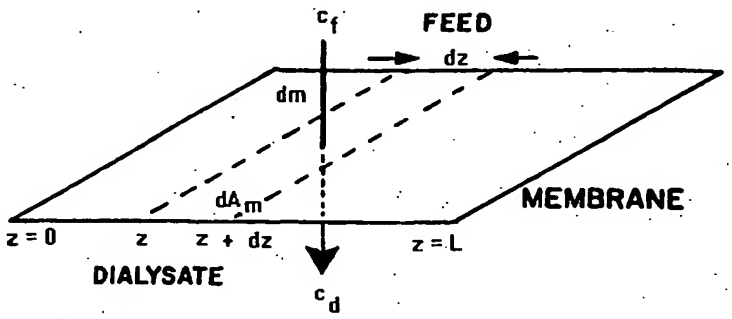

FIGURE 12–8. Diffusive mass transfer across an element of a membrane of length dz and area dA_m (reprinted from Klein, Ward, and Lacey 1987 with permission).

where c_f and c_d are the solute concentrations in the feed and dialysate, respectively, in the element of length dz. Equation (12–41) can be integrated along the length of the membrane to give the following equation for overall solute transfer rate:

$$Q_i = k_o A_m \left(\frac{\Delta c^*_{z=1} - \Delta c^*_{z=0}}{\ln(\Delta c^*_{z=1} / \Delta c^*_{z=0})} \right), \tag{12–42}$$

where $\Delta c^*_{z=0}$ and $\Delta c^*_{z=1}$ are the transmembrane concentration differences at either end of the device. For countercurrent flow, $\Delta c^*_{z=0} = c_{fi} - c_{do}$ and $\Delta c^*_{z=1} = c_{fo} - c_{di}$. This leads to the following equation for overall mass transfer in a dialyzer with this flow configuration:

$$Q_i = k_o A_m \left(\frac{(c_{fo} - c_{di}) - (c_{fi} - c_{do})}{\ln[(c_{fo} - c_{di})/(c_{di} - c_{do})]} \right). \tag{12–43}$$

A similar expression can be derived for cocurrent flow by redefining $\Delta c^*_{z=0}$ and $\Delta c^*_{z=1}$.

If ultrafiltration is negligible, inlet and outlet flows are equal for both the feed and dialysate streams. Using this assumption, the following overall mass balances may be written for each stream:

$$Q_i = Q_f(c_{fi} - c_{fo}) = Q_d(c_{do} - c_{di}). \tag{12–44}$$

The performance of a dialyzer can be described in terms of its *dialysance* D^*, which is defined as the rate of mass transfer divided by the concentration difference between inlet feed and inlet dialysate (Klein, Ward, and Lacey 1987), that is,

$$D^* = \frac{Q_i}{c_{fi} - c_{di}}. \tag{12–45a}$$

Clearance, defined by Eq. (12–45b), is derived from renal physiology and is similar to dialysance except that dialysate solute concentration is not considered (Colton and Lowrie 1981):

$$C = \frac{Q_i}{c_{fi}}. \tag{12–45b}$$

If the solute concentration is zero in the dialysate (as in the case of a single-pass dialysate system), then dialysance and clearance have the same value.

Combining Eqs. (12–43), (12–44), and (12–45a), the following expression is obtained for the dialysance of a countercurrent dialyzer in terms of membrane properties and hydrodynamics (k_o, A_m) and operating conditions (Q_f, Q_d):

$$D^* = Q_f \left(\frac{\exp[k_o A_m (1 - Q_f/Q_d)/Q_f] - 1}{\exp[k_o A_m (1 - Q_f/Q_d)/Q_f] - Q_f/Q_d} \right). \tag{12–46}$$

Note that if the feed and dialysate flows are essentially equal ($Q_f \cong Q_d$), then

$$D^* = Q_f \frac{k_o A_m}{Q_f + k_o A_m}. \tag{12–47}$$

The foregoing assumes that the solute is distributed freely in the solvent phase. This assumption may not always be valid; for example, in protein solutions, small solutes may bind to the protein molecules and exist in equilibrium between the free and bound states. In such circumstances, modifications of Eq. (12–46) must

be used to determine dialysance (Farrell et al. 1974).

Equation (12–46) can be used to estimate the degree of separation of two solutes by a given dialyzer. For any solute, the extraction ratio E of solute from the feed stream is given by

$$E = \frac{Q_f c_{fi} - (Q_f - Q_{uf})c_{fo}}{Q_f c_{fi}}. \quad (12\text{–}48)$$

For negligible ultrafiltration, this reduces to

$$E = \frac{c_{fi} - c_{fo}}{c_{fi}}. \quad (12\text{–}49)$$

If the inlet concentration of solute in the dialysate is zero ($c_{di} = 0$), Eq. (12–49) further reduces to

$$E = \frac{D^*}{Q_f}. \quad (12\text{–}50)$$

The extraction ratio represents the fraction of maximum solute concentration change that can be attained under a given set of operating conditions. It is analogous to the effectiveness of a heat exchanger. The terms of Eq. (12–46) can be combined through definition of the following dimensionless parameters:

$$N_t = k_o A_m / Q_f, \quad (12\text{–}51)$$

$$Z = Q_f / Q_d. \quad (12\text{–}52)$$

Here N_t is defined as the number of transfer units and is a measure of the mass transfer size of a dialyzer. Extraction ratio E for countercurrent flow can now be expressed as

$$E = \frac{1 - \exp[-N_t(1 - Z)]}{1 - Z\exp[-N_t(1 - Z)]}. \quad (12\text{–}53)$$

Similar expressions can be derived for other flow configurations including well-mixed dialysate flow (Michaels 1966). For cocurrent flow,

$$E = \frac{1 - \exp[-N_t(1 + Z)]}{1 + Z}. \quad (12\text{–}54)$$

For perpendicular flow,

$$E = \left(\frac{1}{N_t Z}\right) \sum_{n=0}^{\infty} [S_n(N_t) S_n(N_t Z)], \quad (12\text{–}55)$$

where

$$S_n(Y) = 1 - \exp(-Y) \sum_{m=0}^{n} \left(\frac{Y^m}{m!}\right).$$

The term "perpendicular flow" refers to the case wherein the feed and dialysate streams flow at 90° relative to each other. This term was chosen instead of "crossflow" because "crossflow" is used interchangeably with "tangential flow" to describe flow tangential to the membrane surface.

The relationships between E, N_t, and Z are shown graphically for each of the three flow configurations in Figures 12–9, 12–10, and 12–11. The separation factor α_{jk} in a dialytic process can be considered to be the ratio of the fractional masses of two solutes removed from their common feed stream, under a given set of operating conditions. By applying Equation (12–48) to each solute, we can see that α_{jk} is equal to the ratio of fractional extractions of the two solutes. Thus, Figures 12–9, 12–10, and 12–11 can be used to estimate the relative separation of two solutes from a knowledge of their overall mass transfer coefficients, membrane area, and feed and dialysate flow rates.

Contribution of Convection to Mass Transfer

The above derivations are based on the assumption that convective mass transfer is negligible; that is, significant ultrafiltration is not occurring. If significant ultrafiltration does occur, mass transfer will be enhanced by the addition of a convective component to the diffusive mass transfer described above. Ultrafiltration will occur from the feed to the dialysate in response to a pressure gradient, which may be either applied, in order to concentrate the feed, or obligatory, as a consequence of the geometry of the device and the desired feed flow rate. Less commonly, if the feed is highly concentrated

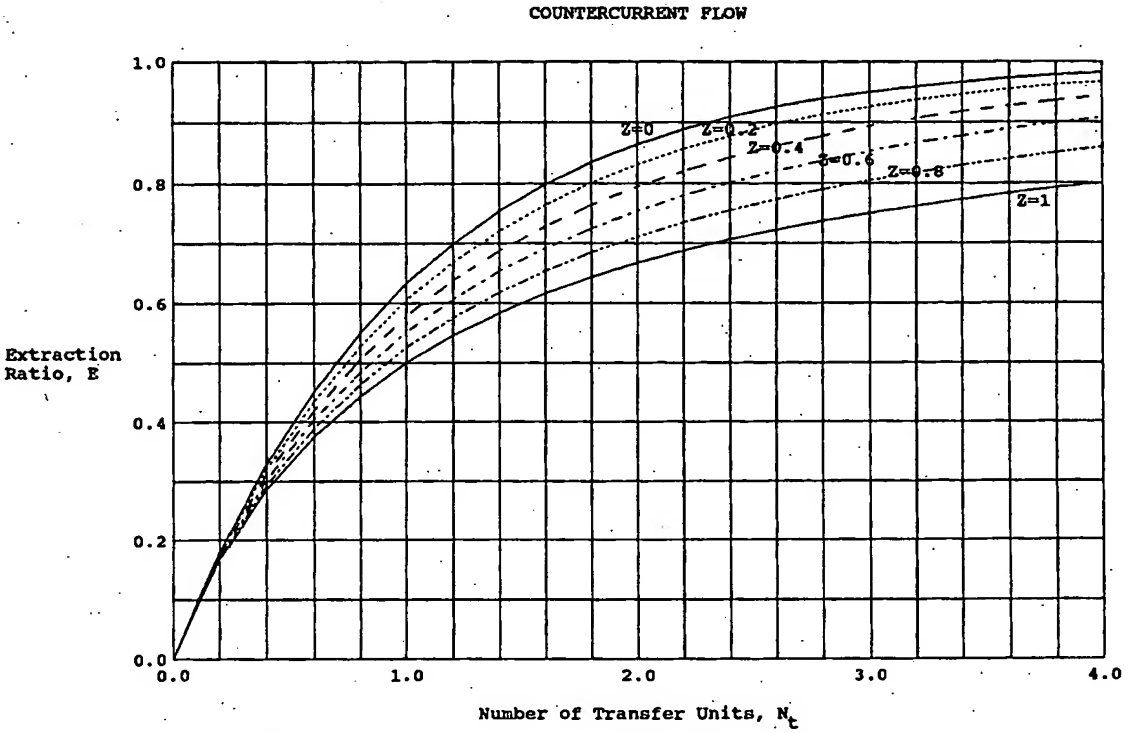

FIGURE 12–9. Extraction ratio E as a function of number of transfer units N_t in a countercurrent flow dialyzer. The graphs of Figures 12–9, 12–10, and 12–11 can be used to estimate the relative separation of two solutes in each of three flow configurations.

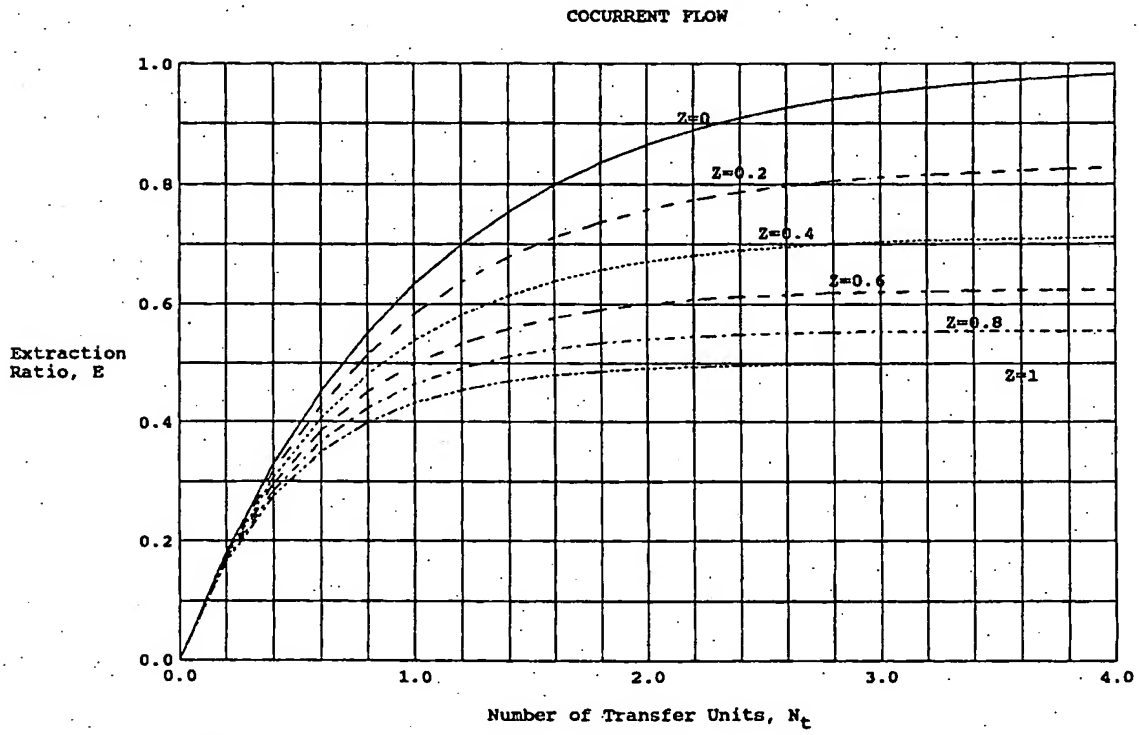

FIGURE 12–10. Extraction ratio E as a function of number of transfer units N_t in a cocurrent flow dialyzer.

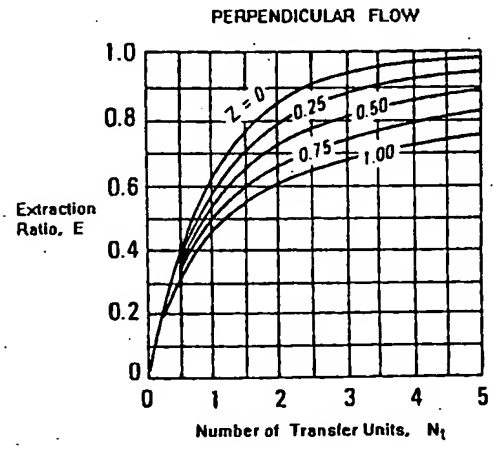

FIGURE 12–11. Extraction ratio E as a function of number of transfer units N_t in a perpendicular flow dialyzer (reprinted from Colton and Lowrie 1981 with permission).

and the dialysate dilute, ultrafiltration may occur from the dialysate to the feed in response to an osmotic gradient. In the first case, ultrafiltration will enhance solute transport while in the second it will impede it.

As discussed earlier, at a steady state the overall solute flux J_s at a point on the membrane can be considered to consist of the sum of a diffusive and convective component:

$$J_s = P_m \Delta c_s + J_v(1 - \sigma)\bar{c}_s, \quad (12\text{–}56)$$

where the first term on the right side, $P_m \Delta c_s$, represents diffusive transfer and the second term, $J_v(1 - \sigma)\bar{c}_s$, convective transfer (Spiegler and Kedem 1966). The average solute concentration within the membrane, $\bar{c}_s$, can be estimated using Eqs. (12–57), (12–58), and (12–59) (Villaroel, Klein, and Holland 1977):

$$\bar{c}_s = c_w - \frac{\Delta c_s}{3}, \quad (12\text{–}57)$$

where c_w is the feedside solute concentration at the membrane wall, which can, in turn, be estimated using concentration polarization theory, of which Eq. (12–58) is an example specific to dialysis:

$$\frac{c_w}{c_f} = \frac{1 + \psi + (1 - \sigma)\xi c_d/c_f}{(1 - \sigma)(1 + \xi) + \psi}, \quad (12\text{–}58)$$

where $\xi = [\exp(\mathrm{Pe}) - 1]^{-1}$ (where Pe is typically <0.1 in dialytic processes) and $\psi = [\exp(\theta) - 1]^{-1}$. For hollow-fiber membranes, θ is given by

$$\theta = 0.709 J_v \left(\frac{z d^3 N}{Q_f D^2}\right)^{0.33}, \quad (12\text{–}59)$$

where z is the axial distance from the hollow-fiber inlet to the point at which c_w is being evaluated.

The relative magnitudes of diffusive and convective transfer are functions of the membrane permeability P_m and the reflection coefficient σ. For species of small molecular size, the resistance to diffusive transfer through a membrane is low, that is, P_m is large, and diffusive transfer always significantly exceeds convective transfer at low Peclet numbers. However, as solute molecular size increases, membrane permeability decreases logarithmically (Farrell and Babb 1973), whereas reflection coefficients increase at a much lesser rate and the relative importance of convection to overall mass transfer increases. This effect is illustrated in the following example.

Figure 12–12 shows the membrane permeability and reflection coefficient as a function of molecular weight for a cellulosic dialysis membrane (Wendt et al. 1979). Consider two solutes, A and B, having molecular weights of 200 and 2000 daltons, respectively, both having feedside concentrations at a point on the membrane surface of 0.1 g/cm^3. Assuming negligible dialysate-side concentrations, $\Delta c_s = 0.1$ g/cm^3 (referring to both solutes). Using Eqs. (12–57), (12–58), and (12–59), an estimate of the value of $\bar{c}_s$ can be made. For both solutes, Eq. (12–58) estimates the value of c_w/c_f to be unity ($c_w \cong c_f$). Then, Eq. (12–57) gives $\bar{c}_s = 0.067$ g/cm^3 for both solutes A and B.

For solute A, $P_m = 3.6 \times 10^{-4}$ cm/s and $1 - \sigma = 0.8$. Substituting these values into Eq. (12–56), the following result is obtained:

$$J_s = (3.6 \times 10^{-5} + 0.054 J_v) \text{ g/s} \cdot \text{cm}^2. \quad (12\text{–}60)$$

As the ultrafiltration rate increases from 0 to 0.5×10^{-4} cm/s, J_s increases from 3.6×10^{-5} g/s·cm^2 to 3.9×10^{-5} g/s·cm^2; that is, convec-

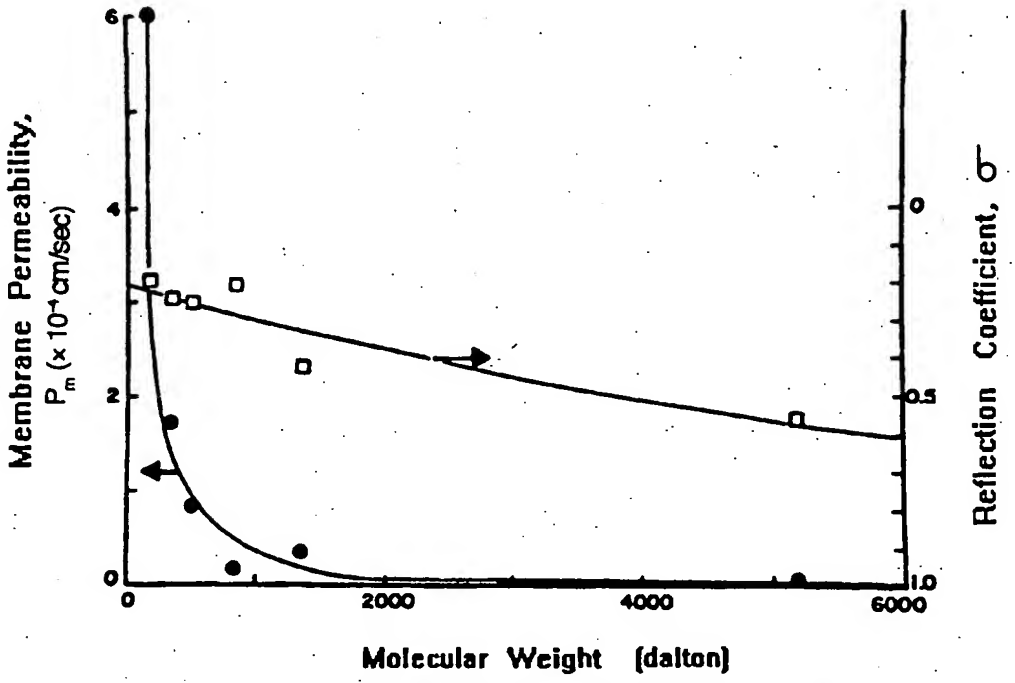

FIGURE 12–12. Membrane permeability and reflection coefficient as a function of solute molecular weight for a typical dialysis membrane (Cuprophan® 150 PM) (after Klein, Ward, and Lacey 1987).

tion increases overall solute transfer by 8%. For solute B, $P_m = 0.40 \times 10^{-4}$ cm/s and $1 - \sigma = 0.6$. Under these conditions, Eq. (12–56) reduces to

$$J_s = (0.40 \times 10^{-5} + 0.04J_v)\ \text{g/s} \cdot \text{cm}^2. \tag{12–61}$$

Now, for an increase in ultrafiltration rate from 0 to 0.5×10^{-4} cm/s, J_s increases from 0.40×10^{-5} to 0.60×10^{-5} g/s·cm^2, an increase in overall mass transfer of 50%.

The above considerations deal with a point on the membrane. Application of these concepts to the dialyzer as a whole requires that the feed and dialysate solute concentrations at every point on the membrane be expressed in terms of known concentrations. Such an approach has been developed by Schindhelm, Farrell, and Stewart (1977), who by assuming a zero inlet dialysate concentration and a linear dialysate concentration profile, developed the following expression for the dialysance of solutes greater than 300 dalton molecular weight in a countercurrent dialyzer in the presence of simultaneous diffusion and convection. [Note that the equations for X and Y given in this reference contain misprints; the correct expressions are as given in Eqs. (12–63) and (12–64).]

$$D^* = \frac{X}{1 + Y}, \tag{12–62}$$

where

$$X = -\frac{k_o A_m + Q_{uf}(1 - \sigma)}{Q_{fi} - Q_{uf}} \frac{Q_{fi}}{Z} [1 - \exp(Z)], \tag{12–63}$$

$$Y = -[k_o A_m + Q_{uf}(1 - \sigma)] \frac{k_o A_m}{Q_{fi} Q_{do} Z^2} \times \left[1 + \left(\frac{Z}{2}\right) + \left(\frac{1}{Z}\right)[1 - \exp(Z)]\right] + \frac{X}{Q_{fi}} + \frac{k_o A_m}{Z Q_{do}}, \tag{12–64}$$

$$Z = \frac{k_o A_m - Q_{uf}\sigma}{Q_{fi}}. \tag{12–65}$$

A similar analysis, but one that requires a numerical methods solution, has been described by Jaffrin, Gupta, and Malbranq (1981).

The contribution of convection to overall mass transfer, illustrated previously for a point on the membrane, can now be estimated for the dialyzer as a whole. Referring to the previous example, consider the contribution of convection to dialysance for the two solutes A and B in a dialyzer containing 10^4 cm^2 of cellulosic membrane operating in a countercurrent configuration with feed and dialysate flow rates of 8 and 16 cm^3/s, respectively. For such a membrane, the overall mass transfer coefficients of solutes A and B are on the order of 3.23×10^{-4} and 0.37×10^{-4} cm/s, respectively, while the reflection coefficients are on the order of 0.2 and 0.4, respectively. Using these data in Eqs. (12–62) through (12–65), we can calculate that the dialysance of solute A will increase by 12% (from 2.47 to 2.78 cm^3/s) as the ultrafiltration rate increases from 0 to 0.5 cm^3/s, while the same increase in ultrafiltration rate will result in an increase of 84% (from 0.36 to 0.66 cm^3/s) in the dialysance of solute B. This example further demonstrates the important contribution of convection to overall mass transfer for larger molecular weight species.

NOTATION

General Notation

See the General Notation section at the beginning of this handbook.

Special Notation

A_m membrane area, L^2
A_p total pore opening area/membrane area, dimensionless
C clearance, L^3/t
d_{ti} inside diameter of the tube or hollow fiber, L
d_{to} fiber outside diameter, L
D^* dialysance, L^3/t
E extraction ratio, dimensionless
k mass transfer coefficient, L/t
K distribution coefficient, dimensionless
l_p pore length, L
L_D diffusional mobility per unit osmotic pressure difference, L/tp
L_{Dp} ultrafiltration coefficient, L/tp
L_p hydraulic permeability, L/tp
L_{pD} coefficient of osmotic flow, L/tp
N molar flux, mol/L^2t
N_i molar flux of species i, mol/L^2t
N_t number of transfer units
P_m diffusive permeability of solute in dialysis, L/t
q ratio of solute radius to pore radius, dimensionless
Q_d dialysate flow rate, L^3/t
Q_f feed flow rate, L^3/t
Q_{uf} ultrafiltration rate from the feed to the dialysate, L^3/t
R mass transfer resistance, t/L
y distance, normal direction, L
z distance, axial direction, L
z^* distance, axial direction, dimensionless
Z ratio of feed to dialysate flow rate, Q_f/Q_d, dimensionless

Greek Letters

η viscosity, M/Lt
σ reflection coefficient defined by Eq. (12–18), dimensionless
ω solute permeability coefficient, mol/L^2tp

Subscripts

d dialysate
o overall
s solute

REFERENCES

Bean, C. P. 1972. The physics of porous membranes—neutral pores. In *Membranes, A Series of Advances, Vol. 1, Macroscopic Systems and Models*, ed. G. Eisenman, pp. 1–54. New York: M. Dekker.

Beck, R. E., and J. S. Schultz. 1972. Hindrance of solute diffusion within membranes as measured with microporous membranes of known pore geometry. *Biochim. Biophys. Acta* 255:273–303.

Bird, R., W. E. Stewart, and E. N. Lightfoot. 1960. *Transport Phenomena*. New York: John Wiley and Sons.

Bungay, P. M. 1986. Transport principles—porous membranes. In *Synthetic Membranes: Science, Engineering and Applications*, ed. P. M. Bungay,

H. K. Lonsdale, and M. N. de Pinho. Dordrecht, Holland: D. Reidel Publishing Company.

Colton, C. K. 1969. Permeability and transport studies in batch and flow dialyzers with applications to hemodialysis. Ph.D. diss. Massachusetts Institute of Technology, Cambridge, MA.

Colton, C. K. 1988. Unpublished data.

Colton, C. K., and E. G. Lowrie. 1981. Hemodialysis: physical principles and technical considerations. In *The Kidney*, Vol. II, ed. B. M. Brenner and F. C. Rector, Jr., pp. 2425–2489. New York: W. B. Saunders Company.

Colton, C. K., K. A. Smith, P. Stroeve, and E. W. Merrill. 1971. Laminar flow mass transfer in a flat duct with permeable walls. *AIChE J.* 17: 773.

Cooney, D. O., E. J. Davis, and S.-S. Kim. 1974. Mass transfer in parallel-plate dialyzers—a conjugated boundary value problem. *Chem. Eng. J.* 8:213–222.

Crank, J. 1975. *The Mathematics of Diffusion*. Oxford: Clarendon Press.

Davis, H. R., and G. V. Parkinson. 1970. Mass transfer from small capillaries with wall resistance in the laminar flow regime. *Appl. Sci. Res.* 22:20.

Farrell, P. C., and A. L. Babb. 1973. Estimation of the permeability of cellulosic membranes from solute dimensions and diffusivities. *J. Biomed. Mater. Res.* 7:275–300.

Farrell, P. C., J. W. Esbach, J. E. Vizzo, and A. L. Babb. 1974. Hemodialyzer reuse: estimation of area loss from clearance data. *Kidney Int.* 5:446–450.

Gostoli, C., and A. Gatta. 1980. Mass transfer in a hollow-fiber dialyzer. *J. Membr. Sci.* 6:133–149.

Happel, J. 1959. Viscous flow relative to arrays of cylinders. *AIChE J.* 5:174–177.

Hermans, J. J. 1978. Physical aspects governing the design of hollow-fiber modules. *Desalination* 26:45–62.

Jaffrin, M. Y., B. B. Gupta, and J. M. Malbrancq. 1981. A one-dimensional model of simultaneous hemodialysis and ultrafiltration with highly permeable membranes. *J. Biomech. Eng.* 103:261–266.

Jagannathan, R., and U. R. Shettigar. 1977. Analysis of a tubular hemodialyzer—effect of ultrafiltration and dialysate concentration. *Med. Biol. Eng. Comput.* 15:134–139.

Katchalsky, A., and P. F. Curran. 1965. *Nonequilibrium Thermodynamics in Biophysics*. Cambridge, MA: Harvard University Press.

Katchalsky, A., and O. Kedem. 1962. Thermodynamics of flow processes in biological systems. *Biophys. J.* 2(suppl.):53.

Kedem, O., and A. Katchalsky. 1958. Thermodynamic analysis of the permeability of biological membranes to nonelectrolytes. *Biochim. Biophys. Acta* 27:229.

Keller, K. H. 1973. *Fluid Mechanics and Mass Transfer in Artificial Organs*. Special publication by *Trans. Am. Soc. Artif. Intern. Organs*. Washington, DC: Georgetown University Press.

Klein, E. 1977. Hollow-fiber membrane developments. *J. Appl. Polym. Sci.* 31:361–381.

Klein, E., F. F. Holland, and K. Eberle. 1979. Comparison of experimental and calculated permeability and rejection coefficients for hemodialysis membranes. *J. Membr. Sci.* 5:173–188.

Klein, E., R. A. Ward, and R. E. Lacey. 1987. Membrane processes—dialysis and electrodialysis. In *Handbook of Separation Process Technology*, ed. R. W. Rousseau. New York: John Wiley and Sons.

Lévêque, J. A. 1928. Les lois de la transmission de chaleur par convection. *Ann. Mines* 13:201, 305, 381.

Michaels, A. S. 1966. Operating parameters and performance criteria for hemodialyzers and other membrane-separation devices. *Trans. Am. Soc. Artif. Intern. Organs* 12:387–392.

Noda, I., and C. C. Gryte. 1979. Mass transfer in regular arrays of hollow fibers in countercurrent dialysis. *AIChE J.* 25:113–122.

Onsager, L. 1931a. Reciprocal relations in irreversible processes. I. *Phys. Rev.* 37:405–426.

Onsager, L. 1931b. Reciprocal relations in irreversible processes. II. *Phys. Rev.* 38:2265–2279.

Prasad, R., and K. K. Sirkar. 1988. Dispersion-free solvent extraction with microporous hollow-fiber modules. *AIChE J.* 33:177–188.

Renkin, E. M. 1954. Filtration, diffusion, and molecular sieving through porous cellulose membranes. *J. Gen. Physiol.* 38:225.

Schindhelm, K., P. C. Farrell, and J. H. Stewart. 1977. Convective mass transfer in the artificial kidney. Paper read at 2nd Australian Conference on Heat and Mass Transfer, 16–18 February 1977, University of Sydney.

Sparrow, E. M., and A. L. Loeffler, Jr. 1959. Longitudinal laminar flow between cylinders arranged in regular array. *AIChE J.* 5:325–330.

Spiegler, K. S., and O. Kedem. 1966. Transport

coefficients and salt rejection in uncharged hyperfiltration membranes. *Desalination* 1: 311–326.

Spriggs, H. D., and N. N. Li. 1976. Liquid permeation through polymeric membranes. In *Membrane Separation Processes*, ed. P. Meares. Amsterdam: Elsevier Scientific Publishers.

Staverman, A. J. 1951. Theory of measurement of osmotic pressure. *Rec. Trav. Chim.* 70: 344.

Vemiory, A., R. DuBois, P. Decoodt, J. P. Gassee, and P. P. Lambert. 1973. Measurement of the permeability of biological membranes. Application to the glomerular wall. *J. Gen. Physiol.* 62:489–507.

Villaroel, F., E. Klein, and F. Holland. 1977. Solute flux in hemodialysis and hemofiltration membranes. *Trans. Am. Soc. Artif. Intern. Organs* 23:225–233.

Wendt, R. P., E. Klein, E. H. Bressler, F. F. Holland, R. M. Serino, and H. Villa. 1979. Sieving properties of hemodialysis membranes. *J. Membr. Sci.* 5:23–49.

Wilson, E. E. 1915. A basis for rational design of heat transfer apparatus. *Trans. ASME* 37:47.

Yang, M.-C., and E. L. Cussler. 1986. Designing hollow-fiber contactors. *AIChE J.* 32:1910–1916.

Yasuda, H., A. Peterlin, C. K. Colton, K. A. Smith, and E. W. Merrill. 1969. Permeability of solutes through hydrated polymer membranes. III. theoretical background for the selectivity of dialysis membranes. *Die Makromol. Chemie* 126:177–186.

Yasuda, H., C. E. Lamaze, and L. D. Ikenberry. 1968. Permeability of solutes through hydrated polymer membranes. I. diffusion of sodium chloride. *Die Makromol. Chemie* 118:19–35.

Yasuda, H., C. E. Lamaze, and A. Peterlin. 1971. Diffusive and hydraulic permeabilities of water in water-swollen polymer membranes. *J. Polym. Sci.* 9:1117–1131.

Membrane Handbook

Edited by

W. S. Winston Ho, Ph.D.

and

Kamalesh K. Sirkar, Ph.D.

VNR VAN NOSTRAND REINHOLD
New York

Disclaimer

To the best of the authors' and publisher's knowledge, the information contained in this handbook is accurate. However, the publisher and authors assume no responsibility nor liability for any consequences arising from the use of the information contained herein. Final determination of the suitability of any information for use contemplated by any user is the sole responsibility of the user. In addition, the citation of commercial products, tradenames, or names of manufacturers is not to be construed as an endorsement or recommendation for use.

Library of Congress Catalog Card Number 91-43661
ISBN 0-442-23747-2

Manufactured in the United States of America

Published by Van Nostrand Reinhold
115 Fifth Avenue
New York, NY 10003

Chapman and Hall
2-6 Boundary Row
London, SE1 8HN, England

Thomas Nelson Australia
102 Dodds Street
South Melbourne 3205
Victoria, Australia

Nelson Canada
1120 Birchmount Road
Scarborough, Ontario MIK 5G4, Canada

16 15 14 13 12 11 10 9 8 7 6 5 4 3 2 1

Library of Congress Cataloging-in-Publication Data

Membrane handbook/editors, W. S. Winston Ho and Kamalesh K. Sirkar.
p. cm.
Includes index.
ISBN 0-442-23747-2
1. Membranes (Technology)—Handbooks, manuals, etc. I. Ho, W. S. Winston, 1943- , II. Sirkar, Kamalesh K., 1942-
TP159.M4M4444 1992
660'.2842—dc20

91-43661
CIP

13

Design

Stephen B. Kessler
Sepracor Inc.

Elias Klein
University of Louisville

MEMBRANE SELECTION

Membrane Materials

When a dialysis membrane separates two aqueous phases, the problem of material choice is relatively simple. Clearly, the membrane pores must be filled with water during use, so wettability is a primary consideration. As a consequence of this requirement, the predominant materials for dialysis membranes are relatively hydrophilic polymers. At one end of the spectrum are cellulose and poly(ethylene-co-vinyl alcohol) (Eval), and on the other end poly(methylmethacrylate), the latter prewetted by the manufacturer. In between fall cellulose acetate with a degree of substitution (DS) of 2.5, poly(acrylonitrile-co-methallylsulfonic acid), and other acrylonitrile copolymers.

The use of poly(ethersulfone) membranes (PES) for hemodialysis would appear to be a contradiction to the wettability requirement, but many dialyzers made from this material contain a small amount of poly(vinylpyrrolidone) (PVP) as an alloying agent to the PES. The PVP provides the requisite wetting, although there may still be very small diameter pores that are inactive during dialysis because of the exclusion of water.

The membrane in widest use for dialysis is regenerated cellulose. It can be produced by a variety of means, but two processes dominate. The oldest and most widely used process is based on producing a copper amine complex of cellulose in a strongly alkaline solution (i.e., the cuprammonium process). The solution containing 5 to 8% cellulose is coagulated by dissociating the complex and removing excess copper and alkali. The characteristics of membranes produced by this process are very high wet strengths, very thin membranes (as thin as 0.0005 cm), and a uniform cross section. A second process for producing cellulose mem-

branes relies on casting a cellulose acetate membrane from a high-temperature solvent. The resulting cellulose acetate membrane is then hydrolyzed to de-acetylate the polymer to the native cellulose. Because cellulose acetate polymers are generally lower in molecular weight than the cellulose used in the cuprammonium process, these membranes have lower strength and stability to alkali.

The cellulose membranes are atypical in that they contain a high percentage of water, yet do not lose their mechanical integrity. As will be shown later, this high water content correlates with rapid solute diffusivity within the membrane.

When the membrane separates two differing and immiscible phases, the material selection must reflect which phase is to be the pore wetting phase (see Chapter 41 for further details). Thus, if the dialytic process is to remove an organic acid from an organic solvent by extraction with an aqueous base, a lipophilic membrane might be chosen. The organic phase would wet the pores preferentially to the aqueous phase and transfer would occur at the aqueous/membrane interface. The organic layer in the membrane would become depleted and must then be considered as a major contributor to the boundary layer. If, instead, a hydrophilic membrane were selected, the membrane would be wet with the aqueous phase (see Chapter 41 for alternative wetting conditions) and transfer would occur at the organic/membrane interface. Now the salt of the organic acid would accumulate in the membrane structure until it is carried away by the aqueous phase. The boundary layer problem is then reversed. A knowledge of the relative membrane diffusivities, i.e., organic acid in organic solvent in the membrane *vis-à-vis* organic salt in the aqueous membrane phase, would aid in predicting the preferred choice of membrane material.

In either of the above cases, the membrane material would have to be completely resistant to the solvent effects of either phase. Absence of solubility is not a sufficient criteria. Many membrane structures are produced as metastable phases that very slowly undergo compaction of their structure to more stable forms. If the contacting solvent accelerates this process, the membrane life may be shortened such that practical applications are impossible.

Finally, the various fabrication options available with a given material must be considered. Most current dialysis devices are produced in the form of hollow fibers or tubes. Materials formed by sintering are difficult to produce in long lengths such as are required by tubes. Thus, the preponderance of membranes available today is produced by coagulating a melt, or solution, or a suspension via some extrusion process. Because diffusion paths should be kept short, dialytic membranes are generally less than 0.0050 cm thick. Such thin walls coupled with a need to wind, or bend, the tubes dictates that the materials must have relatively high tensile moduli. Consideration of these factors, together with an understanding of the phase-separation mechanisms that lead to semipermeable structures, is what constitutes the art and science of "membranology."

Membrane Structures

Membrane morphology provides important distinctions between dialytic membranes. For simple dialysis applications, such as equilibration of microsolute concentrations in two aqueous phases, the choices are many. Most dialytic membranes have pore radii of $>15 \times 10^{-8}$ cm, which is significantly larger than the Stokes radius of a 500-dalton molecular weight solute. However, when selective separation of solutes is desired, other constraints apply. Dialytic membranes with pore radii in the 75×10^{-8}–100×10^{-8}-cm range are now available. The sieving properties of such membranes allow them to retain macromolecules while selectively removing solutes of "middle" molecular weight. These "high-efficiency" dialysis membranes typically exhibit high levels of protein adsorption, which makes *a priori* prediction of selectivity problematic.

Since device clearance, in the absence of significant ultrafiltration, depends on short diffusion paths within the membrane, the thinner

the membrane, the more rapid the mass transfer. So the first choice would be to make a membrane as thin as the material will allow, while still providing the requisite mechanical stability for potting and pumping pressures. In addition to being thin, the membrane must provide the required morphology, i.e., porosity and pore size. These are often conflicting demands. High porosity implies reduced load-bearing elements in the cross section and, thus, limited tensile strengths. Fortunately, the more hydrophilic materials, such as cellulose and copolymers of vinyl alcohol, can be produced as thin, highly efficient hydrogel membranes reinforced by crystalline regions. The more hydrophobic, glassy polymers, such as poly(sulfones), are produced in asymmetric form to provide a thin solute-resistant skin supported by a more porous substructure. The thick substructure provides the mechanical support needed.

The ability to produce membranes composed of a solute-retentive skin integral with a more porous substructure was a major development in membrane technology. This asymmetric structure was found to permit production of membranes with large L_p values that were still retentive to small molecules. The major benefit of this asymmetry, however, accrues to ultrafiltration and reverse osmosis membranes since the substructure does not produce a stagnant boundary layer in such convective processes. With dialysis membranes, the thickness of the porous substructure can add significantly to the boundary layer problems by producing an unstirred layer of fluid. Such layers create unwanted transport resistances.

Asymmetric membrane structures are produced by the coagulation process used to convert a solution of polymer into a membrane structure. The phase-separation mechanisms that occur as the polymer is precipitated from concentrated solutions include liquid-liquid and liquid-gel transitions. The skin is thought to be caused by a rapid loss of solvent from the polymer solution film into the coagulating bath. The resulting highly concentrated polymer solution precipitates with a morphology different from the underlying polymer solution since the initially coagulated surface acts as a barrier to transfer of the solvent out of—and nonsolvent into—the lower layers of the solution. For the production of asymmetric dialysis membranes, the control of such phase-separation mechanisms becomes rather critical because of the added demand for thin cross sections in dialytic applications.

Table 13–1 lists some commercially available, hollow-fiber dialysis membranes with their basic performance parameters. Both gel-type and asymmetric membrane structures are represented. Unless otherwise noted, UFR (ultrafiltration rate per membrane area) and P_m (diffusive permeability) were measured using saline solutions.

MEMBRANE MODULES

Module Types

Industrial Dialyzers

Early industrial dialyzers comprised three general configurations: the tank type, the plate-and-frame type, and the tube type. Tuwiner (1962) reviews these designs as well as those of early laboratory dialyzers in considerable detail. Of the three types, the plate-and-frame design was most widely used, while the tube type (a bundle of tubular membranes) did not achieve commercial importance.

The Cerini dialyzer, an example of the tank design, was developed in Italy in 1928 to reclaim sodium hydroxide in the rayon industry. It consisted of a $3 \times 1.5 \times 1.2$-m tank, containing 50 membrane bags totaling 300 m^2 of membrane area. Thus, the membrane area per unit volume of this dialyzer was 55 m^{-1}. Each of the cotton bags was supported by an internal metal mesh frame and was individually connected to the water supply. Feed solution flowed into the tank at the bottom and exited at the top by simply overflowing.

The patent literature abounds with examples of plate-and-frame (or filter press) dialyzer designs (Tuwiner 1962). By providing improved membrane support compared to the tank design, these dialyzers allowed the use of much thinner membranes. The lower diffusive resistance of

TABLE 13–1. Performance Parameters of Some Representative Hollow-Fiber Dialysis Membranes.

Description	Material	UFR (mL/h m² mm Hg)	P_m/Vitamin B_{12} (10^{-3} cm/min)
Cuprophan® C1 (Enka)	Cellulose	4.0	5.3
Cuprophan® D4 (Enka)	Cellulose	3.0	4.0
Highflux® RC-HP400 (Enka)	Cellulose	30	12
Gambro HF	Cellulose	3.8[a]	4.8
Hospal	PAN-methallyl sulfate	27	9.5
Baxter/Toyoba	Cellulose acetate	4.6	5.7
Fresenius F-6	Polysulfone	4.6	5.9
Fresenius F-60	Polysulfone	33	17
Toray/Hoechst	PMMA	16[a]	10

[a]Values measured from whole blood.

the thin membranes led to a fivefold to tenfold increase in productivity per unit membrane area relative to the Cerini dialyzer. On a membrane area per unit volume basis, plate-and-frame and tank-type dialyzers were comparable.

One of the more recent examples of the plate-and-frame design is the Graver dialyzer. This design uses a poly(vinylchloride) membrane support frame. A "repeat unit" in such a dialyzer consists of two such frames—one perfused with dialysate and one with feed solution—two sheets of membrane, and the necessary gaskets. The Graver dialyzer is comprised of 150 such units. Figure 13–1 illustrates a single-repeat unit in a generic plate-and-frame dialyzer.

In countercurrent operation, the lower density dialysate flows downward and the higher density feed flows upward in adjacent compartments. Thus, the increasing density of the dialysate as solute is transferred to it and the corresponding decrease in density of the feed both serve to facilitate a balanced flow distribution among the cells. Hydrostatic pressure in the dialysate cells is maintained at a higher level than in the feed cells, which ensures that the membranes are pressed against the support structure of the feed frames.

The hollow-fiber dialyzer, developed first for hemodialysis, has been adapted for industrial applications. Enka AG offers industrial dialyzers based on their Cuprophan® regenerated cellulose hollow-fiber membrane. Hollow fibers of 200-μm inside diameter and 16-μm wall thickness are interwoven with thread and grouped into bundles. Three such bundles are contained in the annular space between two stainless steel tubes and encapsulated with polyurethane at each end, which forms tubesheets. The inner tube acts as a conduit feeding the shell side of the module, the flow exiting at one end of the outer tube. Two such submodules of 28-cm effective fiber length are joined in series, comprising a module of 22.5-m² membrane area. The membrane area per unit volume of this device is approximately 2200 m^{-1}, which is a fortyfold increase over the tank or plate-and-frame designs.

While the traditional aqueous/aqueous dialysis process is limited in its industrial applications, modern hollow-fiber dialyzers with expanded chemical resistance are finding new application in aqueous/organic solvent extraction processes. An example of an industrial hollow-fiber device of this kind is produced by Sepracor Inc. (more details are available in

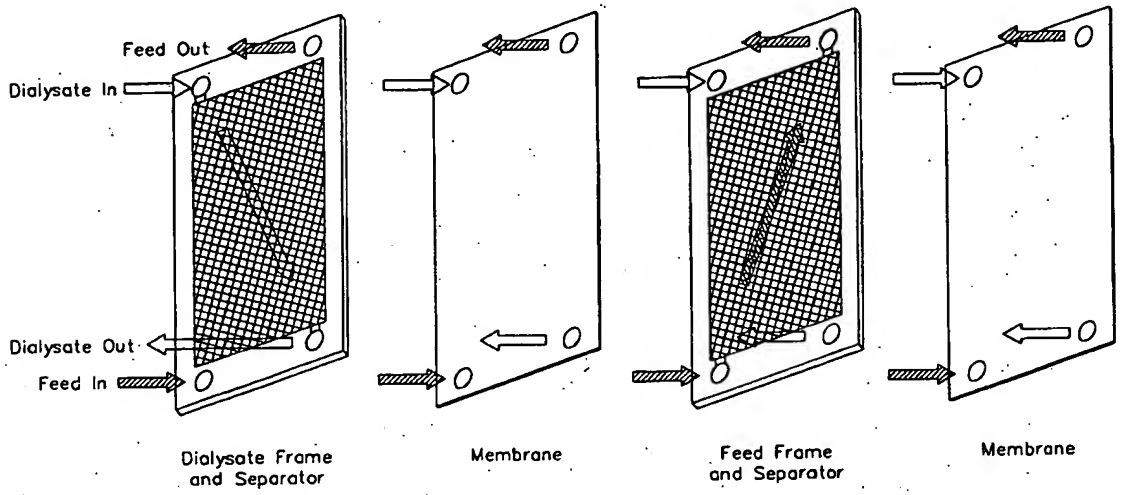

FIGURE 13–1. Single-repeat unit from a typical plate-and-frame dialyzer (with gaskets omitted).

Chapter 41). These modules were developed specifically for applications involving aqueous/nonaqueous extraction processes and are fabricated from materials that are resistant to organic solvents. Available hollow-fiber types include regenerated cellulose and poly(acrylonitrile), both of 200-μm inside diameter. The fibers are encapsulated in epoxy, forming a cartridge that has ends provided with radial O-ring seals. The cartridge is installed in a housing, together comprising a module. Sepracor modules are sized by total available fiber packing volume and range from 1.5 mL to 12 L in size (Figure 13–2). A 12-L module packed with typical regenerated cellulose dialysis fibers has a membrane area of 65 m^2. Based on overall volume occupied, its membrane area per unit volume is comparable to the Enka unit described above.

Hemodialyzers

As described in Chapter 11, Kolff and Berk (1944) demonstrated the feasibility of hemodialysis and applied the process clinically using a "rotating drum" artificial kidney. This device consisted of a drum wrapped with cellulose sausage casing through which blood flowed while the drum was rotated in a bath of dialysate solution.

In 1956 Kolff and coworkers developed the

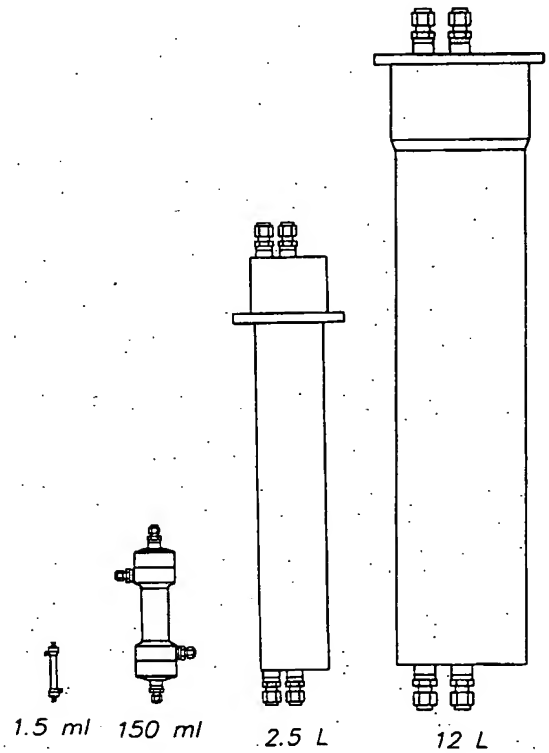

FIGURE 13–2. Hollow-fiber modules for diffusion-based membrane separation processes. The modules are sized by total fiber packing volume and range from lab scale (1.5 mL) to production scale (12 L). (Courtesy of Sepracor Inc.).

coil dialyzer. Like the rotating drum, this design was based on a tubular cellophane membrane. The tubing was flattened and rolled into a coil along with a sheet of plastic mesh. In operation, blood flowed inside of the cellophane tubing around the coil, while dialysate flowed axially through the space formed by the plastic mesh.

Kiil introduced a plate-and-frame hemodialyzer in 1960. Like industrial plate-and-frame modules, it was operated in the countercurrent flow mode. It was a reusable device whose membranes were replaced by disassembly and reassembly of the unit. Due to the amount of labor required to maintain reusable dialyzers, disposable devices of both the coil type and plate-and-frame type were introduced (Figure 13–3). The disposable designs tend to be more compact than their reusable counterparts and are sold presterilized. Hollow-fiber hemodia-

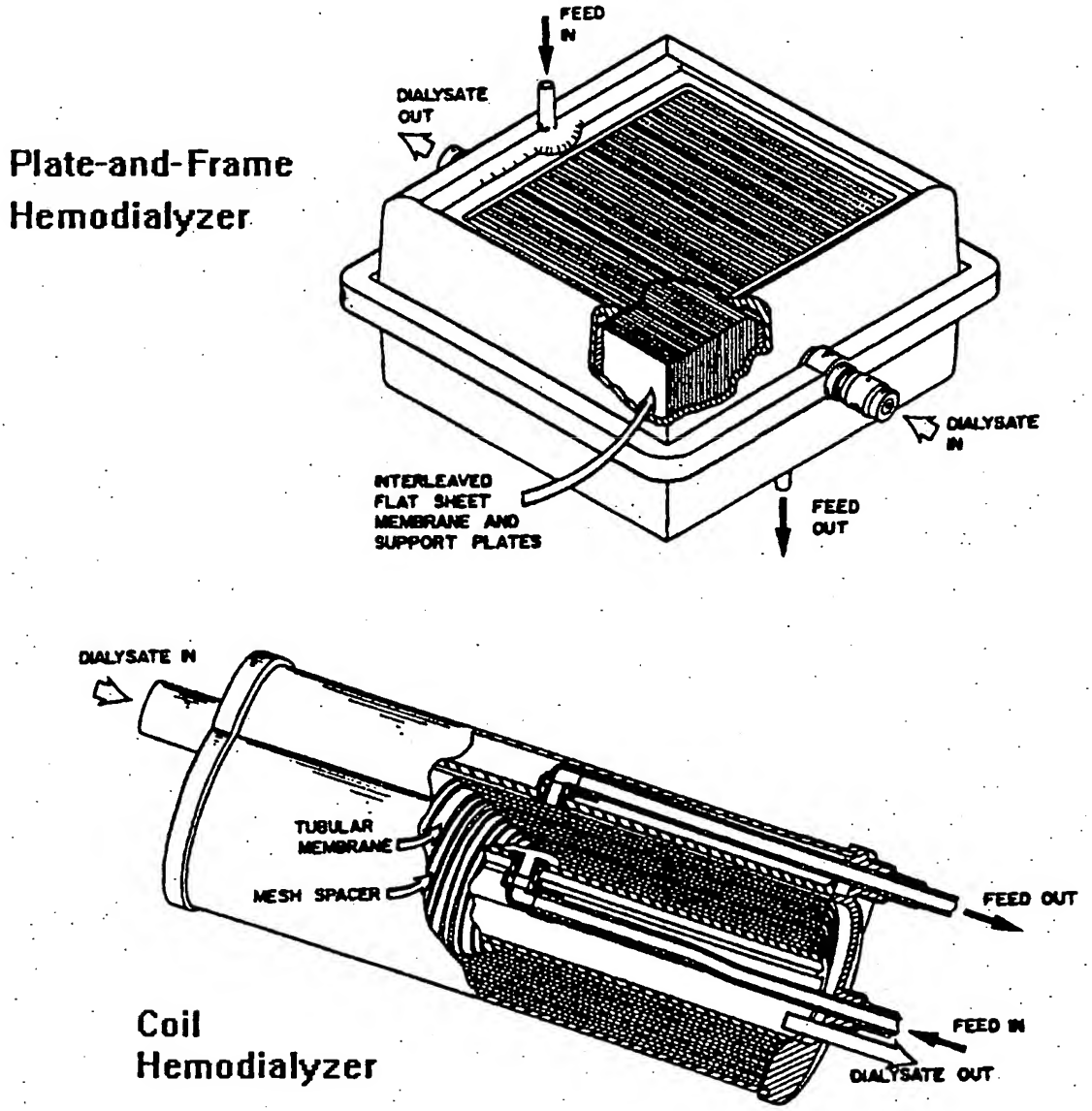

FIGURE 13–3. Hemodialyzers of the coil type and plate-and-frame type (Courtesy of Baxter Healthcare Corp.; Klein, Ward, and Lacey 1987).

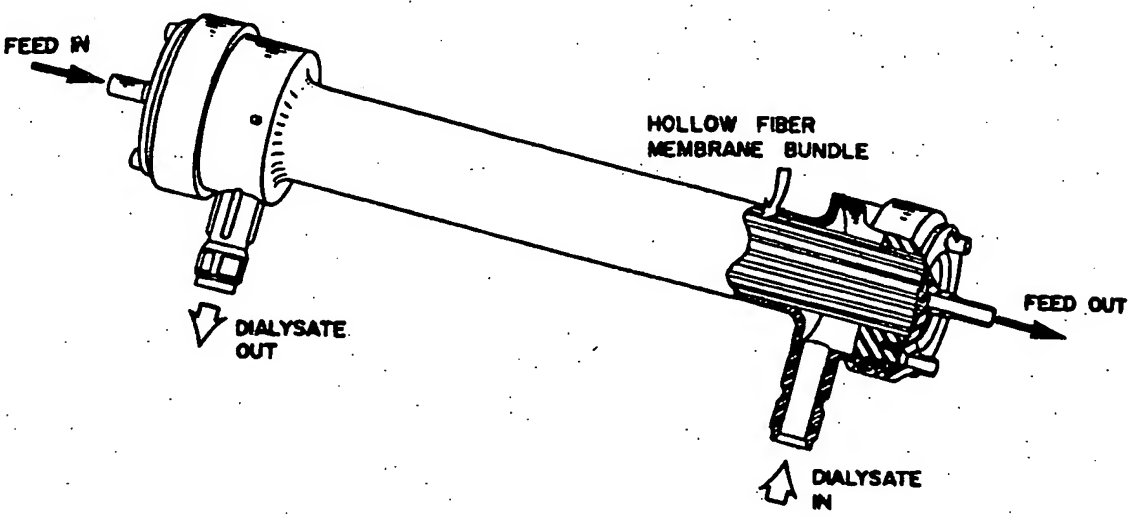

FIGURE 13–4. Typical hollow-fiber hemodialyzer (Courtesy of Baxter Healthcare Corp.; Klein, Ward, and Lacey 1987).

lyzers were first introduced in 1966 (Lipps et al. 1967). The structure of a typical unit is shown in Figure 13–4. A bundle of hollow fibers is contained in a housing and encapsulated at each end forming tubesheets. At each end, a gasket and endcap form headers to direct blood flow in and out of the lumens of the fibers. Adjacent to each tubesheet is a circumferential header, which directs dialysate flow in and out of the shellside space. The device is geometrically similar to a shell-and-tube heat exchanger.

The housing and endcaps of these modules are usually fabricated from a transparent engineering polymer such as polycarbonate or poly(styrene-co-acrylonitrile). The encapsulant that forms the tubesheet is typically a polyurethane, and a low-Durometer elastomer such as silicone rubber is used for the gasket between the endcap and tubesheet.

The hollow-fiber dialyzer has achieved widespread acceptance and has largely supplanted other designs. This is due to the ease with which this design can be manufactured, its compactness, and its reliable performance in extracorporeal systems. While originally intended as disposable items, health care costs have provided incentive to reuse these dialyzers, but only with respect to a single patient.

Module Design

From a design standpoint, the evolution of dialyzer types followed two distinct lines: those intended for industrial applications and those intended for medical applications. Specific examples from both application areas were given in the preceding section.

Many of the design requirements of utmost importance to membrane devices intended for medical use have no relevance to industrial membrane modules (and vice versa). For example, all hemodialyzers are packaged sterile and are intended for single use or reuse only with the same patient. Examples of presterilized industrial membrane devices exist; however, they are the exception and no presterilized industrial dialyzers are known to the authors. The converse is equally true. An industrial dialyzer that utilizes an organic solvent as extractant and is to be periodically cleaned with sodium hydroxide must be constructed from chemically resistant materials, unlike those used for medical devices.

Scale is another obvious difference. Membrane devices intended for medical use are designed to perform mass transfer operations at a scale dictated by human anatomy and physiology. Industrial dialyzers, on the other hand, are

scaled according to process economic factors and are typically much larger than their medical counterparts.

Process economics, in addition to affecting scale, also tends to favor long-lived industrial dialyzers, while, as mentioned above, hemodialyzers are intended for single use or limited reuse. The economics of health care as applied to end-stage renal disease (ESRD) is equally important in determining hemodialyzer design—no "overdesign" is tolerated in this cost-conscious and competitive market.

To illustrate the process leading to an optimized module design, a hollow-fiber module will be designed for a hypothetical dialysis process. As described in the preceding sections, hollow-fiber modules have become prevalent in both industrial and medical applications due to their high volumetric efficiency and ease of manufacture.

The hypothetical process for which this hollow-fiber module is being designed is an industrial process in which the product is a compound of 20K-dalton molecular weight ($\bar{M}$) in aqueous solution. It is desired to separate this product from a contaminant whose molecular weight is 200 dalton in a continuous process. The product solute concentration is 5 g/L and required productivity is 50 kg/h. The contaminant concentration is 1 g/L and should be reduced to 0.1 g/L or less by the process. An aqueous dialysate solution is to be used, which is buffered to pH 7.0.

Fiber Dimensions and Number

Yang and Cussler (1986) conclude that the key advantage of hollow-fiber membrane modules is the high ratio of membrane area to unit device volume they provide and that mass transfer coefficients for hollow-fiber devices are, in general, similar to those for other types of equipment. This conclusion provides a clue regarding choice of fiber dimensions—minimization of fiber diameters (inside and outside diameters) maximizes area-to-volume. However, practical lower limits exist for fiber diameters. The internal diameter is limited by the size of any suspended particles that may be present. Wall thickness, which together with inside diameter determines outside diameter, has a lower limit set by fiber strength requirements.

For given diameters, fiber length has an upper limit that is determined by pressure drop and/or mass transfer parameters. In the case of high-flux membranes, excessive translumenal pressure drop (TLP) causes high ultrafiltration rates, the effects of which are discussed in Chapter 12. A further consequence of high TLP is the increased likelihood of Starling's flow or back-filtration, which can cause a further decrease in separation efficiency. If, at the maximum lumenal flow rate allowable within TLP limitations, the desired degree of solute transfer occurs in less than one pass of the feed stream, then fiber length is excessive. At the other extreme, if too short a device is designed, excessively high flow rates are required to achieve a given value of k_o over a given membrane area and recirculation may be required to provide sufficient residence time. Another limit on "shortness" is manufacturing cost. The shorter a device is for a given membrane area, the more potential membrane area is lost to waste and the more expensive the housing becomes.

While not all of these optimization parameters can be included in a single expression, the ones that relate directly to fluid dynamics and mass transfer performance can be dealt with on a quantitative basis. Referring to the hypothetical process described above, based on throughput alone, the minimum feed flow rate required to process 50 kg/h is $Q_f = 10{,}000$ L/h. Assume that the feed solution viscosity is 1.0 cp and that the maximum permissible TLP is 75 kPa (11 psi), relative to the effective fiber length (excluding fiber encapsulated in the tubesheets). Equation (13–1) gives the number of hollow fibers required to process a given feed flow rate within TLP limitations:

$$N = 8\eta L Q_f/(\mathrm{TLP}\pi r_{ii}^4), \qquad (13\text{–}1)$$

where η is solution viscosity, L is effective fiber length, Q_f is feed flow rate, and r_{ii} is fiber internal radius.

A further constraint on the number of fibers required is the membrane area needed to provide a sufficiently high rate of transfer of the contaminant. By choosing commercially available dialysis fibers covering a range of dimensions, practical values of both fiber dimensions and permeability can be assumed. Enka AG offers dialysis fibers of 100, 200, and 300 μm inside diameter (dry dimensions), designated C3, C1, and D4, respectively. Based on the experience of the authors (Klein et al. 1976, 1977), these fibers will be assumed in the wet state to have inside diameters of 125, 250, and 375 μm and wall thicknesses of 22, 22, and 32 μm, respectively.

To a first approximation, the diffusive permeabilities of all three fibers chosen are the same for low molecular weight solutes (<200 dalton) (Klein et al. 1976; 1977). It is assumed throughout the following analysis that passage of the 20K-dalton product is negligible through the membranes chosen. A convenient way of estimating required membrane area (for a first iteration of the design) is to refer to clearance values published for hemodialyzers of a given size. Figure 13–5 gives a value of $C = 90$

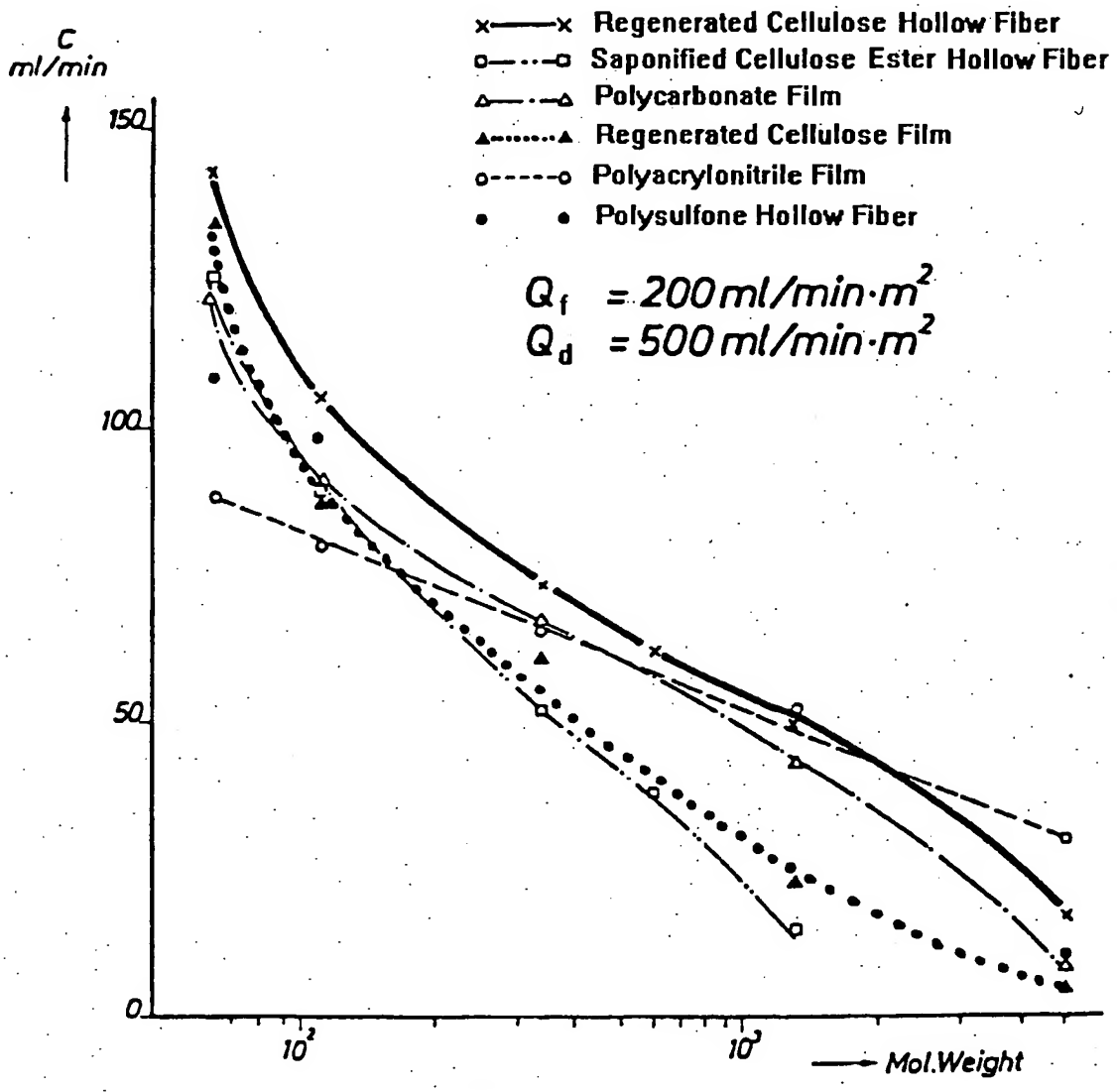

FIGURE 13–5. Clearance of various dialysis membranes as a function of molecular weight (after Enka AG 1982).

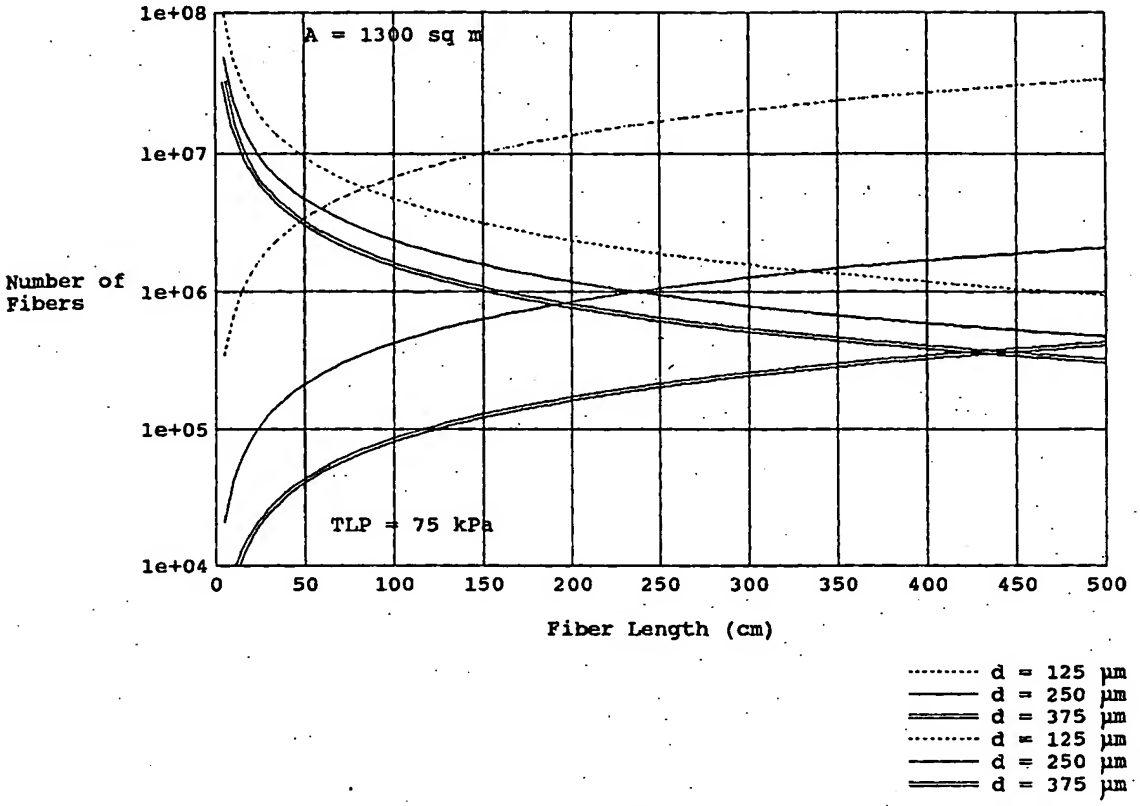

FIGURE 13–6. Number of fibers required as a function of fiber dimensions for constant translumenal pressure drop and area. (Used in designing a hollow-fiber dialysis module for a hypothetical process.)

mL/min for a 1-m^2 dialyzer using one of the hollow fibers chosen above. Dividing Q_f by C gives an estimate of required membrane area, $A_m = 1850$ m^2. Equation (13–2) gives the number of hollow fibers required to provide a given membrane area as a function of fiber dimensions:

$$N = A_m/(2\pi r_{ti}L). \qquad (13\text{–}2)$$

Figure 13–6 was plotted to illustrate how the above constraints of TLP and membrane area limit the design space for the fibers chosen. The three curves that originate in the lower left corner of the graph were generated by Eq. (13–1) using the above-stated values for TLP and Q_f — each curve represents a different fiber inside diameter. Values of fiber number and length on or above each of the curves result in acceptable TLP values that are below 75 kPa.

The family of curves that originates in the upper left corner of the graph were generated by Eq. (13–2) with $A_m = 1850$ m^2. Values of fiber number and length on or above these curves result in membrane areas that are sufficient for mass transfer. Thus, for the 125-μm-i.d. fiber, greater than 10^7 fibers are required for most fiber lengths. The minimum number occurs at the intersection point of the two curves: $L = 85$ cm and $N = 5.6 \times 10^6$ fibers. For the 250-μm-i.d. fiber, the minimum number is $N = 1.0 \times 10^6$ at a fiber length of $L = 240$ cm. The corresponding values for the 375-μm-i.d. fiber are $N = 3.6 \times 10^5$ and $L = 440$ cm. At this point in the design process, it would be premature to select from among the three fiber sizes. A detailed evaluation of mass transfer performance may help in the decision.

Flow Configurations

Feed and dialysate flows can be either cocurrent or countercurrent in the case of parallel flows.

Other possibilities discussed in Chapter 12 include well-mixed dialysate and perpendicular flow. Of these possible flow configurations, countercurrent and perpendicular flow offer the best potential mass transfer performance. Cocurrent operations are indicated when minimal convective flow is desired and obligatory pressure drops are encountered. Under cocurrent flow configurations, pressure differences are easier to balance across the membrane along the length of the device. Countercurrent flows are used to maximize concentration differences between the inlet dialysate and the outlet feed, where the latter is most dilute.

Based on Eqs. (12–53) through (12–55), extraction ratio E versus the number of transfer units N_t has been plotted for three of the four flow configurations discussed above. Figures 12–9 through 12–11 of Chapter 12 show these plots of the countercurrent, cocurrent, and perpendicular flow cases. Extraction ratio E is perhaps the most meaningful measure of dialyzer mass transfer performance. In countercurrent flow, at equal values of N_t and Z, somewhat higher values of E are obtained than in the other two flow configurations. This implies that countercurrent flow is the most efficient of the three configurations. Recall, however, that $N_t = \bar{k}_o A_m / Q_f$. Thus, comparison at equal values of N_t implies that (if A_m and Q_f are to be held constant) $\bar{k}_o$ is the same in both countercurrent and perpendicular flow hollow-fiber modules operating at the same Q_d. This is most often not the case and $\bar{k}_o$ is usually higher for the perpendicular flow case.

Yang and Cussler (1986) compared published heat transfer correlations for flow external to tubes in both the parallel and perpendicular flow configurations. They further conducted oxygen transfer experiments with hollow-fiber modules in which external water flow in both flow configurations was tested under conditions where membrane resistance was negligible. Figure 13–7 compares the published correlations as well as the correlations

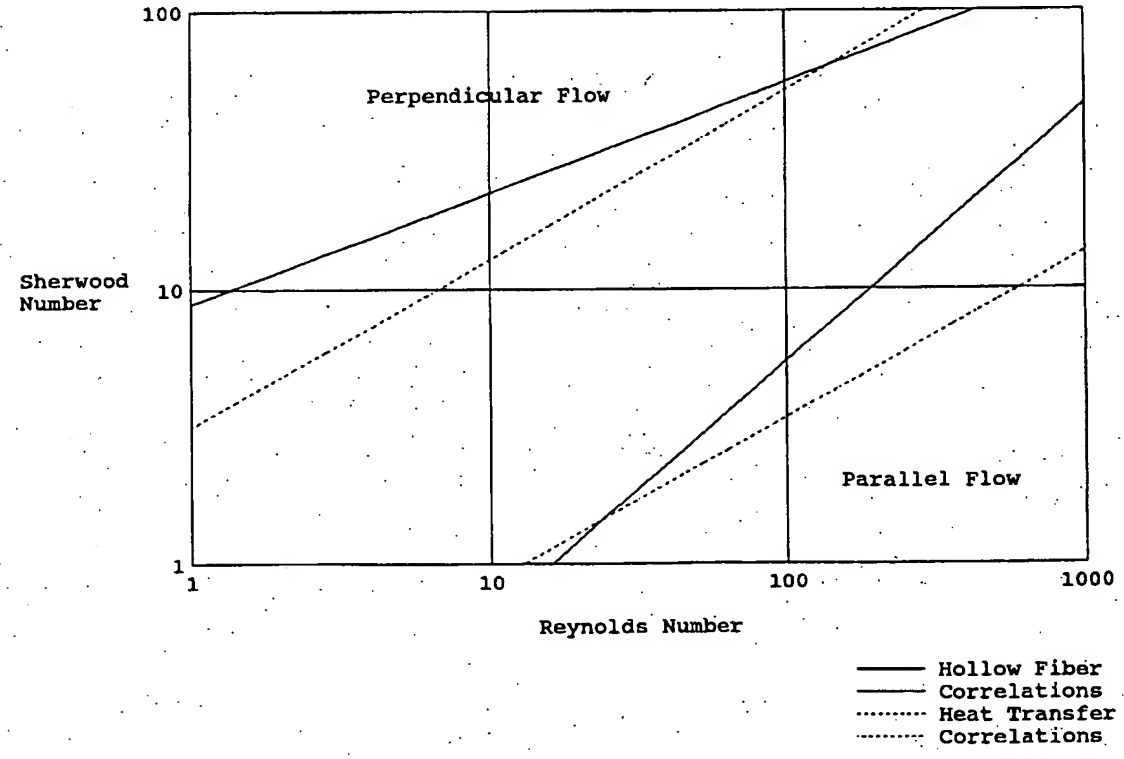

FIGURE 13–7. Mass transfer and heat transfer correlations for flow external to tubes, comparing parallel flow and perpendicular flow.

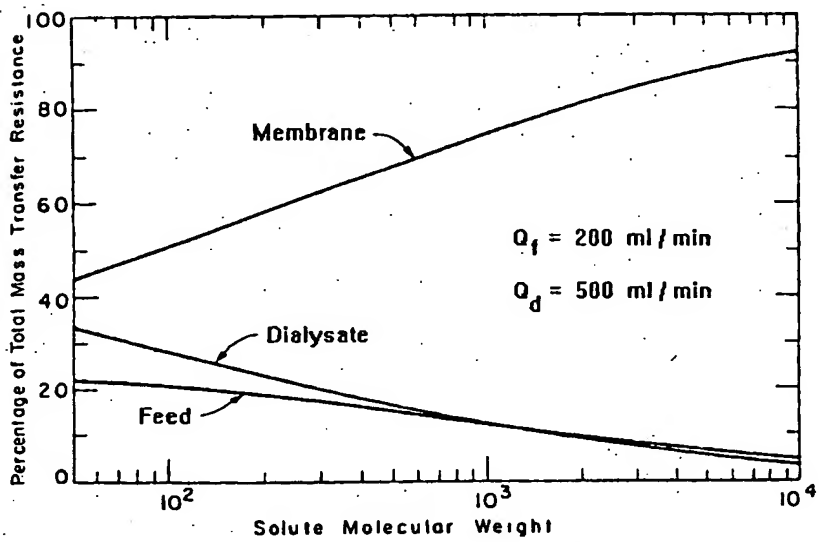

FIGURE 13–8. Relative contributions of feed, membrane, and dialysate mass transfer resistances for a typical hollow-fiber dialyzer operating in countercurrent flow (reprinted from Colton and Lowrie 1981 with permission).

resulting from their experiments. In both cases, the Sherwood number at a given value of Reynolds number is more than an order of magnitude higher in perpendicular flow compared to parallel flow.

Consider the case in which membrane mass transfer resistance is significant, which is more relevant to dialysis. Figure 13–8 shows relative contributions of feed, membrane, and dialysate resistances as a function of solute molecular weight for a typical hollow-fiber dialyzer operating in countercurrent flow. For a solute of 200 dalton $\tilde{M}$, R_d contributes about 25% of the overall mass transfer resistance. Applying the results from Yang and Cussler (1986) for perpendicular flow, a dialyzer containing the same fiber as in Figure 13–8, but with dialysate in perpendicular flow, should show a 25% decrease in R_o due to R_d becoming negligible.

By applying the above example to the plots of Figures 12–9 and 12–11 of Chapter 12, $\bar{k}_o$ (perpendicular) is equal to $1.33\bar{k}_o$ (parallel) at the same Reynolds number and comparison should be made between the perpendicular flow case at a value of N_t that is 33% higher than that used in the countercurrent flow case. Compared in this way, for a value of $Z = 0.5$, perpendicular flow attains $E = 0.9$ at $N_t = 5$, while, for countercurrent flow at the same Reynolds number, $N_t = 3.75$ and $E = 0.9$. When enhanced dialysate mass transfer in perpendicular flow is taken into account, perpendicular flow and countercurrent flow are predicted to give comparable overall mass transfer performance in a typical dialytic process.

Shellside Pressure Drop

Another consideration in choosing between perpendicular and countercurrent flow is shellside pressure drop. The above mass transfer comparison was done at equal Reynolds numbers, which is an appropriate basis for a pressure drop comparison as well. Happel's (1959) free-surface model predicts pressure drops for laminar flow relative to arrays of cylinders. He states that his model shows good agreement with experimental results (on arrays of cylinders) up to Re = 100. Referring to the Reynolds number definition, Eq. (12–35) of Chapter 12, the Reynolds number for shellside flow is obtained by inserting fiber outside diameter for the characteristic length L in Eq. (12–35) of Chapter 12. The wet outside diameters for the three hollow fibers chosen are 170, 295, and 440 μm. Thus, at Re = 100, average velocities in the shell for the three fiber sizes are v = 59, 34, and 23 cm/s, respectively. The free-surface model should be applicable since actual hollow-fiber modules are likely to operate below these velocities.

Application of the free-surface model (Happel 1959) to a moderately packed ($\Phi = 0.5$) triangular array of the 295-μm-o.d. fibers gives

resulting values for Darcy's constant of $K_D = 1.18 \times 10^{-6}$ cm^2 for perpendicular flow and $K_D = 3.06 \times 10^{-6}$ cm^2 for parallel flow in the same array [$K_D = \eta v/(\Delta p/l)$]. Since K_D is inversely proportional to pressure drop per unit length, the model predicts a pressure drop that is 2.6 times as large for perpendicular flow as for parallel flow over the same length. However, most practical hollow-fiber module configurations have axial lengths that exceed their transverse flow dimension by factors greater than 2.6:1. Thus, at this level of analysis, comparable pressure drops would be expected for parallel and perpendicular flow.

Keep in mind that the free-surface model applies to rigid, regularly arranged cylinders and that real hollow fibers may deviate significantly. Hermans (1978) compares results predicted by the free-surface model for perpendicular flow with an empirical study using hollow fibers (Dandavati, Doshi, and Gill 1975) and concludes that measured pressure drops exceeded those predicted by the model by a factor of 5:1. Deviations in the direction of higher-than-predicted pressure drops can be attributed to packing of fibers in response to flow, deformation of fibers due to the pressure gradient, nonuniform outside diameter, and "kinkiness." The first two of these causes apply specifically to the perpendicular flow case. Packing of fibers can be controlled by weaving them into a mat or providing local support with supplementary fibers. "Kinkiness," which may increase pressure drop in parallel flow, can be of benefit in perpendicular flow to control packing. In general, the pressure drop behavior in parallel flow is more predictable than in perpendicular flow, and simple fiber bundle configurations (e.g., without weaving or supplementary fibers) give good performance.

For the reasons stated above, the parallel flow regime will be chosen for the module being designed. Predictability, simplicity of design, and module-to-module consistency are good reasons to choose parallel flow for a dialysis process. However, for processes in which one of the fluid boundary layers contributes most of the overall mass transfer resistance, perpendicular flow should be considered. For example, for the experiments conducted by Yang and Cussler (1986), both membrane resistance and gas-phase boundary layer resistance were quite small compared with liquid-phase boundary layer resistance. In this case, perpendicular flow gave overall mass transfer coefficients that exceeded those for parallel flow by more than an order of magnitude, as described in the preceding section.

Prediction of Overall Mass Transfer Performance

Use of Figures 12–9 and 12–11 of Chapter 12 to estimate values for the extraction ratio requires knowledge of a dialyzer's overall mass transfer coefficient $\bar{k}_o$. An experimentally determined value of $\bar{k}_o$ for the solute, membrane, and dialyzer configuration of interest is to be preferred. Estimates of $\bar{k}_o$ can be made based on knowledge of the geometry and fluid dynamics of the dialyzer and the nature of the membrane and solute. Methods have been described in Chapter 12 and this chapter that allow estimation of P_m, $\bar{k}_f$, and $\bar{k}_d$ for a variety of situations. Regardless of whether an experimental measurement or a calculated estimate of $\bar{k}_o$ is used, it is important to make the determination at the projected operating temperature because of the strong temperature dependence of solute diffusivity.

As discussed earlier, the overall mass transfer resistance ($\bar{R}_o = 1/\bar{k}_o$) can be considered the sum of the individual boundary layer and membrane resistances; that is, as shown in Eq. (12–25) of Chapter 12:

$$1/\bar{k}_o = 1/\bar{k}_f + 1/P_m + 1/\bar{k}_d.$$

If the individual mass transfer coefficients can be estimated, then a value for $\bar{k}_o$ can be derived from Eq. (12–25) of Chapter 12. Since three examples of hollow-fiber membranes have been selected, published data can be used as a prediction of P_m. Such studies have been done by Klein et al. (1976, 1977). By interpolation from the results of these studies, P_m for 125- and 250-μm-i.d. fibers, both of which have 22-μm wet wall thicknesses, is estimated to be 4.0 ×

10^{-4} cm/s for a solute of 200 daltons $\bar{M}$ and the 375-μm-i.d. fiber, which has a wall thickness of 32 μm, has an estimated permeability of 3.1×10^{-4} cm/s.

Before attempting to predict $\bar{k}_d$, a value for packing density should be chosen. Noda and Gryte (1979) predicted $\Phi = 0.63$ as the optimum value for packing density, but they, as well as Yang and Cussler (1986) and Hermans (1978), warn of the effect of channeling on shellside mass transfer. If shellside flow is poorly distributed among the fibers, then relatively stagnant regions exist that severely compromise mass transfer. Yang and Cussler observed this effect in a close-packed module that exhibited flow-independent mass transfer at 1/10 the rate of the same fibers in a loosely packed module. The value of Φ at which channeling becomes a problem is dependent on module design factors, such as fiber bundle configuration (woven or unsupported), shell inside diameter and ratio of fiber length to outside diameter. Of course, it is desirable to approach $\Phi = 0.63$ to maximize both surface-to-volume ratio of the module and mass transfer coefficient per unit flow rate. The authors' experience has been that packing densities in the 50 to 60% range can be achieved without undue channeling provided the fiber length is large in proportion to both fiber and shell diameters. The initially proposed fiber lengths arrived at in Figure 13–6 certainly qualify. Therefore, $\Phi = 0.55$ will be chosen as a reasonable value for the design at hand.

To estimate $\bar{k}_d$, a correlation developed by Wald, Kessler, and Lopez (1990) will be used. The basis for this correlation was a series of experiments using a number of identical hollow-fiber modules with L/d much larger than hemodialyzers, which tends to minimize channeling. Mass transfer performance of this series of modules showed little module-to-module variation. Equation (13–3) gives the correlation

$$\overline{\mathrm{Sh}}_d = 0.025\ \mathrm{Re}^{0.94}\ \mathrm{Sc}^{0.33}. \qquad (13\text{–}3)$$

This correlation is similar to that reported by Yang and Cussler (1986) for their loosely packed hollow-fiber modules. Equation (13–3) predicts higher values for the Sherwood number, especially for large values of L/d, than does the Yang and Cussler correlation. The value of exponent b is similar in both correlations (0.94 and 0.93) and is difficult to explain in relation to laminar flow in bundles of rigid tubes. However, this value is typical of shellside mass transfer in hollow-fiber modules (Colton 1988). The fact that this exponent is much higher than predicted or observed for laminar flow in well-defined ducts and higher even than that observed for turbulent flow can be explained if we consider the freedom that hollow fibers have to move laterally and orient with the flow field. As fluid velocity increases in parallel flow, the resulting forces on the fibers tend to improve the uniformity of fiber distribution, which, in turn, minimizes channeling and improves overall mass transfer.

In estimating $\bar{k}_d$ for the module being designed, a value of 1100 is estimated for the Schmidt number (based on a diffusion coefficient of 9×10^{-6} cm^2/s for a 200-dalton solute). The Reynolds number will be calculated for each of the three "minimum fiber number" points selected in Figure 13–6, assuming a feed flow rate of 10,000 L/h and a dialysate flow rate of 20,000 L/h. Then a value for $\overline{\mathrm{Sh}}_d$ is calculated using Eq. (13–3) and $\bar{k}_d$ is calculated using Eq. (12–27) of Chapter 12. The results of these calculations are tabulated in Table 13–2.

Now the fluid-side mass transfer coefficient based on logarithmic mean concentration difference can be estimated. First, inserting the above estimates of membrane permeability and dialysate-side mass transfer coefficient into Eq.

TABLE 13–2. Values of Reynolds Number and Dialysate-Side Sherwood Number and Mass Transfer Coefficient Corresponding to Minimum Fiber Numbers of Figure 13–6.

Fiber Outside Diameter (μm)	Re	$\overline{\mathrm{Sh}}_d$	$\bar{k}_d$ (cm/min)
170	9.0	2.0	0.064
295	29	6.0	0.11
440	55	11	0.13

TABLE 13–3. Values of Wall Sherwood Number and Dimensionless Length Used to Determine Feedside Sherwood Numbers.

Fiber Inside Diameter (μm)	Sh_w	z^*
125	0.40	1.2
250	0.91	0.61
375	1.1	0.40

(13–4), values for k_w can be calculated for each of the fiber diameters:

$$1/k_w = 1/P_m + 1/\bar{k}_d. \qquad (13\text{–}4)$$

Then, an estimate can be made for the wall Sherwood number, as defined by Eq. (12–31) of Chapter 12, at each fiber inside diameter. Values for dimensionless length z^* can be calculated for the minimum fiber number conditions for each of the three fibers. The above results are tabulated in Table 13–3.

Referring to Figure 12–5 of Chapter 12, values of feedside (lumen-side) Sherwood numbers can be determined from the curves. Feedside mass transfer coefficient $\bar{k}_f$ can then be calculated. Overall mass transfer coefficients can now be determined by adding each of the mass transfer resistances previously determined (reciprocal of each k). These values can be found in Table 13–4.

By comparing the values of membrane permeability and the various mass transfer coefficients as resistances (their reciprocals), the relative contributions to overall resistance can be obtained, as shown in Table 13–5.

To reiterate, the initial design compares the three different fibers at equivalent feed and dialysate flow rates, membrane area, and TLP, operating in countercurrent flow. The membrane area was chosen by approximating overall mass transfer using clearance data for a dialyzer containing one of the fibers chosen. Feed flow rate was chosen as the minimum flow required to provide the required throughput of product, and dialysate flow rate was arbitrarily set at twice the feed flow. From Figure 13–6, conditions were chosen such that the minimum total fiber number for each diameter was selected.

The result, as presented in Table 13–5, is favorable in that for all fibers selected, the sum of feed and dialysate resistances contributes only one-third of overall resistance, the rest being contributed by the membrane.

Further insight into the performance of this design and its optimization can be gained by referring to Figure 12–9 of Chapter 12, the plot of extraction ratio versus the number of transfer units for countercurrent flow. Calculating values of N_t for the three fiber diameters can now be done using the $\bar{k}_o$ values in Table 13–4. These values have been referred to a value of $Z = 0.5$ in Figure 12–9 of Chapter 12 and the results are tabulated in Table 13–6.

These extraction ratio values predict that the initial design conditions will result in between 67 and 75% removal of low molecular weight contaminants, depending on the membrane selected. Since the goal is 90% removal, some adjustments must be made in module design and/or operating conditions to achieve a higher extraction ratio.

At this point, the 375-μm-i.d. fiber will be dropped from consideration due to its lower level of performance (which is due primarily to its thicker wall and resulting lower membrane permeability). With the two remaining fibers, simply increasing dialysate flow rate will in-

TABLE 13–4. Feedside Sherwood Numbers and Mass Transfer Coefficients and Overall Mass Transfer Coefficients.

Fiber Inside Diameter (μm)	$\overline{Sh}_f$	$\bar{k}_f$ (cm/min)	$\bar{k}_o$ (cm/min)
125	4.3	0.19	0.016
250	4.3	0.093	0.016
375	4.3	0.062	0.013

TABLE 13–5. Contributions of Feed, Membrane, and Dialysate Resistances to R_o in Initial Design.

Fiber Inside Diameter (μm)	$\bar{R}_f$ (%)	R_m (%)	$\bar{R}_d$ (%)
125	8	67	25
250	17	68	15
375	21	69	10

crease extraction ratio. An increase from 20,000 to 40,000 L/h will approximately double the values of $\bar{k}_d$ associated with each fiber (since $\bar{k}_d$ depends on $Re^{0.94}$). Referring again to Figure 12–9 of Chapter 12, a further advantage results from increasing Q_d, reflected in the choice of $Z = 0.25$, which gives higher extraction ratio values for a given value of N_t. The new values are shown in Table 13–7.

While the changes have brought performance closer to the goal of $E = 0.9$, further increases in Q_d will not achieve the goal. Instead, membrane area will be increased by increasing the total number of fibers, while holding fiber length constant. The value of Q_f will remain unchanged, resulting in a decrease in TLP and in $\bar{k}_f$. If the total fiber number is increased by 50%, A_m will increase to 2775 m^2 and TLP will decrease from 75 to 50 kPa. Since feedside mass transfer is already operating in the asymptotic region of Figure 12–5 of Chapter 12, the decrease in $\bar{k}_f$ will be negligible. Dialysate flow rate will be increased by an additional 50% to maintain the same Reynolds number as in the previous example. Since Q_f has not increased, $Z = 0.17$ in this example. The resulting values of N_t and E (from Figure 12–9 of Chapter 12) are given in Table 13–8.

TABLE 13–6. Number of Transfer Units N_t and Extraction Ratio E for the Initial Design with $Z = 0.5$.

Fiber Inside Diameter (μm)	N_t	E
125	1.8	0.75
250	1.8	0.75
375	1.4	0.67

TABLE 13–7. Number of Transfer Units N_t and Extraction Ratio E Reflecting a 2× Increase in Q_d and $Z = 0.25$.

Fiber Inside Diameter (μm)	N_t	E
125	2.0	0.82
250	1.9	0.81

Physical Design of Membrane Modules

Up to this point, a number of hollow fibers operating in parallel have been considered for design purposes, without regard to modularization. Since the total number of fibers is in excess of 10^6 fibers for the process considered above, multiple modules will be required. For the two fibers still under consideration, the total fiber numbers are now 8.4×10^6 and 1.5×10^6 for the 125- and 250-μm fibers, respectively. Considering the different fiber lengths (85 cm for 125 μm and 240 cm for 250 μm), total module volumes can be calculated as well. At $\Phi = 0.55$, for the 125-μm fiber, an internal module volume of 295 L is required, while the design based on the 250-μm fiber requires 445 L. Assuming a maximum shell inside diameter of 25 cm, seven 85-cm-long modules containing the 125-μm fiber or four 240-cm-long modules containing the 250-μm fiber would meet the requirements. While four of the longer modules occupy more total volume than seven of the shorter modules, manifolding of four modules is simpler. Another practical advantage of the

TABLE 13–8. Number of Transfer Units N_t and Extraction Ratio E Reflecting a 1.5× Increase in A_m, a 3× Increase in Q_d, and $Z = 0.17$.

Fiber Inside Diameter (μm)	N_t	E
125	3.0	0.92
250	2.9	0.91

250-μm-i.d. fiber is that it is more resistant to clogging of the lumen.

Configuration of the modules could be similar to a shell-and-tube heat exchanger or a hollow-fiber hemodialyzer (Figure 13–4). Shellside flow distribution to a 25-cm-diameter bundle of 295-μm-o.d. fibers requires special attention, however. Simply providing a baffled circumferential header at each end of the shell would leave an area of stagnation in the center of the bundle. Instead, flow will be introduced through a distribution tube at one end and in the center of the bundle and will exit circumferentially at the opposite end. The Enka and Sepracor industrial hollow-fiber modules described above use examples of this approach.

Materials Selection

For the process described above, the feed is relatively noncorrosive (pH 7.0). Material selection may be determined more by the method used to clean the modules in this case. For cellulose membranes, a sanitizing solution such as glutaraldehyde or peroxyacetic acid is likely to be used. Either 316 stainless steel or an engineering polymer such as polysulfone can be used to fabricate the module housing. The encapsulant used to form tubesheets at either end of the module could be a polyurethane, silicone rubber, epoxy, or a thermoplastic such as polypropylene.

In the situation where either the feed or dialysate is an organic solvent solution, stainless steel is a good choice for the housing, although more solvent-resistant polymers such as nylon can also be used. The list of possible encapsulants should be shortened to epoxy or polypropylene in this case. Elastomeric seals are limited to elastomers specifically selected for a particular solvent, perfluoro elastomers, or fluoro-polymer-coated seals.

If a membrane is selected that allows steaming-in-place (SIP), then only stainless steel should be considered for a housing material with epoxy or, possibly, a thermoplastic as encapsulant. Ethylene-propylene copolymer elastomers (EPR or EPDM) are a good choice for elastomeric seals in contact with steam. Cleaning with caustic solutions requires similar materials choices to SIP. If sodium hypochlorite is to be used as a cleaning agent, then stainless steel is not a good choice for a housing material. One of the engineering polymers would be preferred.

PROCESS AND SYSTEM DESIGN

Batch versus Continuous Operation

Dialysis can be used as a unit operation in two basic configurations: as a batch operation or in continuous mode. Figure 13–9 depicts a schematic of batch dialysis. A reservoir of volume V and feed solute concentration c_f is dialyzed continuously with an inlet concentration equal to c_{di}. The feed and dialysate streams enter the dialyzer with flows of Q_f and Q_d, respectively. The feed stream exiting the dialyzer returns to the reservoir while the spent dialysate is discarded to enter another recovery process. Such a configuration could be used for stripping low molecular weight contaminants from a high molecular weight product. It could also be used to recover a low molecular weight product by catalytic cleavage of a high molecular substrate in the feed reactor. In that event the spent dialysate is processed to recover the prod-

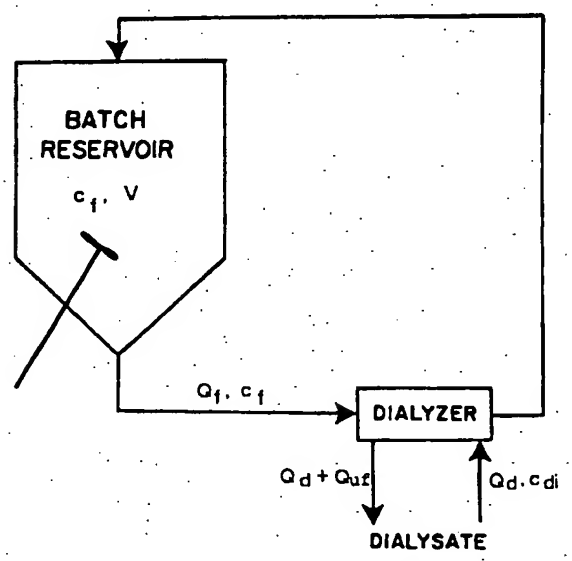

FIGURE 13–9. A batch dialysis process (reprinted from Klein, Ward, and Lacey 1987 with permission).

uct and not discarded. The former represents, in essence, the practice of hemodialysis with the reservoir representing the body pool of water.

A mass balance may be written for the reservoir:

$$\frac{d(Vc_f)}{dt} = -D^*(c_f - c_{di}), \qquad (13\text{–}5)$$

where D^* is the dialysance defined previously. A volume balance may also be written for the reservoir:

$$V = V_0 - Q_{uf}t, \qquad (13\text{–}6)$$

where V_0 is the initial reservoir volume and Q_{uf} is the rate of ultrafiltration from the feed to the dialysate. Substituting for V in Eq. (13–5) leads to

$$(V_0 - Q_{uf}t)\frac{dc_f}{dt} - Q_{uf}c_f = -D^*(c_f - c_{di}). \qquad (13\text{–}7)$$

Rearrangement and integration lead to the following relationship for the reservoir concentration as a function of time:

$$c_f(t) = \frac{D^*c_{di}}{D^* - Q_{uf}}\left(1 - \left(\frac{(V_0 - Q_{uf}t)}{V_0}\right)^b\right) + c_f^0\left(\frac{(V_0 - Q_{uf}t)}{V_0}\right)^b, \qquad (13\text{–}8)$$

where $b = (D^* - Q_{uf})/Q_{uf}$ and c_f^0 is the initial feed solution concentration. If ultrafiltration is negligible, that is, $Q_{uf} = 0$, Eq. (13–5) reduces to

$$V\frac{dc_f}{dt} = -D^*(c_f - c_{di}), \qquad (13\text{–}9)$$

and the reservoir solute concentration is given by

$$c_f(t) = c_f^0 \exp\left(\frac{-D^*t}{V}\right) + c_{di}\left[1 - \exp\left(\frac{-D^*t}{V}\right)\right]. \qquad (13\text{–}10)$$

Dialysis reactors may also be operated in a continuous mode. This can be represented by adding a feed line to the schematic of Figure 13–9.

The addition of a high molecular weight substrate at a flow rate Q_r to an enzymatic reactor whose products permeate the membrane would exemplify one case. As the substrate is converted to dialyzable product at a rate G, the increasing concentration must be incorporated into the previous equations. Equation (13–5) now becomes

$$\frac{d(Vc_f)}{dt} = -D^*(c_f - c_{di}) + G, \qquad (13\text{–}11)$$

and the integrated form incorporates the solute regeneration rate and volume expansion as follows:

$$c_f(t) = \frac{D^*c_{di} + G}{D^* - Q_{uf} + Q_r}\left(1 - \left(\frac{(V_0 - Q_{uf}t)}{V_0}\right)^g\right) + c_f^0\frac{(V_0 - Q_{uf}t)^g}{V_0}, \qquad (13\text{–}12)$$

where

$$g = \frac{D^* - Q_{uf} + Q_r}{Q_{uf} - Q_r}.$$

Staged Operation

To improve the selectivity of a dialytic separation beyond what can be achieved in a single stage, a cascade process consisting of several stages can be used. Rautenbach (1986) has reviewed the cascade process option as it applies to membrane-based processes in general. Noda and Gryte (1981) described a multistaged system with two cross-current dialyzer cascades and a reverse osmosis unit acting as a nonselective solvent stripper. This approach increases the slope of the curves in Figures 12–9, 12–10, and 12–11 of Chapter 12, relating E to N_t, resulting in improved relative separation of two solutes of differing molecular weight. Assuming $Q_f = Q_d$ throughout the system, the extrac-

tion ratio for the system is given by Eq. (13–13):

$$E = \frac{N_t^n}{1 + N_t^n}, \qquad (13\text{–}13)$$

where n is the number of stages in each cascade.

To illustrate the efficacy of this approach in improving selectivity, assume that two solutes, A and B, are being separated in a countercurrent, single-stage dialysis process with $Q_f = Q_d$. Under these conditions, their extraction ratios are $E_A = 0.33$ and $E_B = 0.60$ with $N_{tA} = 0.5$ and $N_{tB} = 1.5$. The resulting selectivity is the ratio of E_B to E_A, which is 1.82. In a three-stage cascade system, Eq. (13–13) predicts E values of 0.11 and 0.77 for a selectivity of 7.0.

NOTATION

General Notation

See the General Notation section at the beginning of this handbook.

Special Notation

A_m membrane area, L^2
c_f^0 initial feed solution concentration, mol/L^3
C clearance, L^3/t
D^* dialysance, L^3/t
E extraction ratio, dimensionless
G conversion rate of the substrate to the dialyzable product, mol/t
k mass transfer coefficient, L/t
K_D Darcy's constant, L^2
N number of hollow fibers
N_t number of transfer units
P_m diffusive permeability of solute in dialysis, L/t
Q_d dialysate flow rate, L^3/t
Q_f feed flow rate, L^3/t
Q_{uf} ultrafiltration rate from the feed to the dialysate, L^3/t
r_{ti} inside radius of hollow fiber, L
R mass transfer resistance, t/L
TLP translumenal pressure drop, p
UFR ultrafiltration rate per membrane area, L/tp
V_0 initial reservoir volume, L^3
y distance, normal direction, L
z distance, axial direction, L
z^* distance, axial direction, dimensionless
Z ratio of feed to dialysate flow rate, Q_f/Q_d, dimensionless

Greek Letters

η viscosity, M/Lt
Φ packing density of a hollow-fiber module, dimensionless

Subscripts

d dialysate
o overall

REFERENCES

Colton, C. K. 1988. Unpublished data.

Colton, C. K., and E. G. Lowrie. 1981. Hemodialysis: physical principles and technical considerations. In *The Kidney*, Vol. II, ed. B. M. Brenner and F. C. Rector, Jr., pp. 2425–2489. New York: W.B. Saunders Company.

Dandavati, M. S., M. R. Doshi, and W. N. Gill. 1975. *Chem. Eng. Sci.* 30:877–886.

Enka AG. 1982. Cuprophan: dialyzing tubular and flat membranes. Product brochure.

Happel, J. 1959. Viscous flow relative to arrays of cylinders. *AIChE J.* 5:174–177.

Hermans, J. J. 1978. Physical aspects governing the design of hollow-fiber modules. *Desalination* 26:45–62.

Klein, E., F. F. Holland, A. Donnaud, A. Lebeouf, and K. Eberle. 1977. Diffusive and hydraulic permeabilities of commercially available cellulosic hemodialysis films and hollow fibers. *J. Membr. Sci.* 2:349–364.

Klein, E., F. F. Holland, A. Lebeouf, A. Donnaud, and J. K. Smith. 1976. Transport and mechanical properties of hemodialysis hollow fibers. *J. Membr. Sci.* 1:371–396.

Klein, E., R. A. Ward, and R. E. Lacey. 1987. Membrane processes—dialysis and electrodialysis. In *Handbook of Separation Process Technology*, ed. R.W. Rousseau. New York: John Wiley & Sons.

Kolff, W. J., and H. T. Berk. 1944. Th artificial kidney: a dialyzer with a great area. *Acta Med. Scan.* 117:121–134.

Lipps, B.
Holme
Oja. 1
Trans.
207.
Noda, I.,
regular
dialysi
Noda, I.,
brane
fractio
meabil
Rautenba
tion. I

Lipps, B. J., R. D. Stewart, H. A. Perkins, G. W. Holmes, E. A. McLain, M. R. Rolfs, and P. P. Oja. 1967. The hollow-fiber artificial kidney. *Trans. Am. Soc. Artif. Intern. Organs* 13:200–207.

Noda, I., and C. C. Gryte. 1979. Mass transfer in regular arrays of hollow fibers in countercurrent dialysis. *AIChE J.* 25:113–122.

Noda, I., and C. C. Gryte. 1981. Multistage membrane separation processes for the continuous fractionation of solutes having similar permeabilities. *AIChE J.* 27:904–912.

Rautenbach, R. 1986. Process design and optimization. In *Synthetic Membranes: Science, Engineering and Applications*, ed. P. M. Bungay, H. K. Lonsdale, and M. N. de Pinho, pp. 457–522. Dordrecht, Holland: D. Reidel Publishing Co.

Tuwiner, S. B. 1962. *Diffusion and Membrane Technology*. New York: Reinhold Publishing Co.

Wald, S. A., S. B. Kessler, and J. L. Lopez. 1990. Characterization of large-scale membrane devices for diffusive transport. Paper read at The International Congress on Membranes and Membrane Processes, 20–24 August 1990, Chicago, IL.

Yang, M.-C., and E. L. Cussler. 1986. Designing hollow-fiber contactors. *AIChE J.* 32:1910–1916.

›wledge support
›n Research and
: Administration
›gy and those of
tors and editors
content of this

S. Winston Ho
ıalesh K. Sirkar

General Notation

Units are given in terms of physical quantities, length (L), mass (M), time (t), temperature (T), amount of substance (mol, mole), electric current (A, ampere), electric potential (V, volt), energy ($E = ML^2/t^2$), and pressure ($p = M/Lt^2$). Special notation is also present in some chapters.

a	activity, various units or dimensionless, or particle radius, L
A	area, L^2
A	species A
A_i	plasticization coefficient for species i, L^3/mol or L^3/M
A_{ij}	interaction coefficient between species i and j, L^3/mol or L^3/M
b	channel height, L, or Langmuir affinity constant, Lt^2/M or p^{-1}, or the ratio of frictional force of solute to the bulk solution, dimensionless
B	species B
B_{ij}	interaction coefficient between species i and j, dimensionless
c	concentration, mol/L^3 [or cm^3 (STP)/cm^3 polymer] or M/L^3
c_{Ai}	concentration of species A at the inside radius of membrane, mol/L^3 [or cm^3 (STP)/cm^3 polymer] or M/L^3
c_{Ao}	concentration of species A at the outside radius of membrane, mol/L^3 [or cm^3 (STP)/cm^3 polymer] or M/L^3
c_H'	Langmuir sorption capacity, L^3 (STP)/L^3 polymer [cm^3 (STP)/cm^3 polymer]
C	heat capacity, L^2/t^2T or E/MT
C_s	reflection constant, 1.14 for air, dimensionless
d	diameter, L
d_f	diameter of filter fibers, L
d_h	hydraulic diameter, L
d_i	inside diameter, or molecular diameter of species i, L
d_o	outside diameter, L
d_p	pore diameter, or particle diameter, L
d_s	stirrer or impeller diameter, L
d_t	tube diameter, L
D	diffusion coefficient, L^2/t
$\hat{D}$	dimensionless diffusivity, $\eta D/r^2\tau_{wo}$
D_0	infinite dilution diffusivity, or characteristic diffusivity, L^2/t
Da	Damköhler number, $k_f c^{n-1} l^2/D$ (n = order of reaction), dimensionless
D_{AB}	diffusion coefficient for solute-carrier complex, L^2/t
D_b	Brownian diffusion coefficient, L^2/t
D_{eff}	effective diffusion coefficient, L^2/t
D_i	diffusivity in the internal phase, L^2/t
D_m	diffusivity in the membrane phase, L^2/t
D_s	shear-induced diffusion coefficient, L^2/t
D_T	thermodynamic diffusion coefficient, L^2/t
E	energy, ML^2/t^2 or E, or activation energy, ML^2/t^2 mol or E/mol, or enhancement factor ($F - 1$), dimensionless
$\Delta\bar{E}_a$	activation energy, ML^2/t^2 mol or E/mol
f	Fanning friction factor, or inertia lift function, dimensionless
f_i	fugacity of component i, M/Lt^2 or p
F	facilitation factor (ratio of flux with carrier present to flux without carrier), dimensionless, or $F = D_H/D_D$, convenient dimensionless group in the dual-mode sorption model
F	Faraday's constant (9.652×10^4 amp · s/g-equivalent), At/g-equivalent
g	gravitational acceleration, L/t^2

g_c	gravitational conversion factor, dimensionless [or ft · lb/(lb force · s^2) in the fps system]
G	Gibbs free energy, ML^2/t^2 or E
GPU	gas permeation unit, 10^{-6} cm^3 (STP)/(cm^2 · s · cm Hg)
H	enthalpy, ML^2/t^2 or E
H	Henry's law constant ($c = Hp$), t^2 mol/L^2M [or cm^3 (STP)/(cm^3 polymer · atm)], or t^2/L^2
H_o	channel half height, L
$\Delta\hat{H}_v$	latent heat of vaporization (per unit mass), L^2/t^2 or E/M
i	electric current density, A/L^2
i_{lim}	limiting current density, A/L^2
I	electric current, A
j	mass transfer or permeation rate, mol/t (or kg-equivalent/s)
j_k	mass transfer rate due to diffusional transport, mol/t (or kg-equivalent/s) or M/t
j_Φ	mass transfer rate due to breakage, mol/t (or kg-equivalent/s) or M/t
J	flux, mol/L^2t or M/L^2t, or volumetric flux, L/t
$\langle J \rangle$	area-averaged volumetric flux, L/t
J_i	flux of species i, mol/L^2t or M/L^2t
$\langle J_L \rangle$	area-averaged volumetric flux from inertial lift model, L/t
$\langle J_s \rangle$	area-averaged volumetric flux from shear-induced diffusion model, L/t
J_v	volumetric flux, L/t
k	thermal conductivity, ML/t^3T or E/LtT, or Boltzmann's constant [1.38×10^{-16} g · $cm^2/(s^2 \cdot °K)$], ML^2/t^2T or E/T, or mass transfer coefficient, L/t
k_f	forward reaction rate constant, (mol/$L^3)^{1-n}/t$, n = order of reaction, various units
k_i	mass transfer coefficient for species i, L/t
k_r	reverse reaction rate constant, (mol/$L^3)^{1-n}/t$, n = order of reaction, various units
K	distribution coefficient, or hydrodynamic constant, dimensionless, or $K=C'_Hb/H$, convenient dimensionless group in the dual-mode sorption model
K_c	cake permeability, L^2
K_{di}	diffusion constant relating diffusivity to concentration for species i, L^5/mol t or L^5/Mt
K_{eq}	equilibrium constant (for extraction reaction), dimensionless or various units
K_i	distribution coefficient for species i, a_i/a'_i, dimensionless
K_{req}	equilibrium constant for stripping or re-extraction reaction, dimensionless or various units
K_s	solubility product, various units, or sorption coefficient, mol/L^3 or M/L^3
K_t	tortuosity correction factor for bubble point, dimensionless
l	membrane thickness, L
L	membrane length, or height of a column extractor, L
LRV	filter log reduction value, dimensionless
m	molal concentration, mol/M
m_i	distribution coefficient for species i, a_i/a'_i, dimensionless
M	mass, M
M	molarity, mol/L^3 (g-mole/liter or kg-mole/m^3)
$\bar{M}$	molecular weight, M/mol
n	number of moles
n_p	number of pores per unit membrane area, L^{-2}
N	number of hollow fibers, or number of emulsion globules
N	normal (g-equivalent/liter or kg-equivalent/m^3)
$\bar{N}$	Avogadro's number, 6.023×10^{23} molecules/mol
Δp	pressure drop, M/Lt^2 or p
p	pressure or partial pressure, M/Lt^2 or p
P	permeability coefficient, various units, or fractional penetration, dimensionless
Pe	Peclet number, vd/D, or v_eL/D_{Le}, dimensionless
q	heat flux, M/t^3 or E/L^2t
Q	flow rate or permeation rate, mol/t or M/t, or volumetric flow rate, L^3/t
Q_e	volumetric flow rate of the external phase, L^3/t
Q_i	volumetric flow rate of the internal phase, L^3/t
Q_m	volumetric flow rate of the membrane phase, L^3/t
Q'	excess p L^2/t
$\hat{Q}$	dimensio
$\hat{Q}_{cr}$	critical formatio
Q_v	volumetr
r	radius, c
r_d	drum rac
r_i	inside ra
r_o	outside radius, l
r_p	pore rad
r_t	tube rad
R	gas cons of solut less
R_c	cake re L^{-1}
$\hat{R}_c$	specific ness, L^-
R'_c	specific M
R_e	electrica
Re	Reynold
R_f	reaction terfacial m^2s)
R_i	rejectior tion par
R_m	membra or L^{-1}
R_{mf}	final me
R_{mi}	initial r
R_r	reaction area, m
s	cake co less
S	entropy for flu geomet
S_c	specific solids v
Sc	Schmid
Sh	Sherwo less
S_m	specific solids v
t	time, t
$t_{1/2}$	half-life

Q'	excess particle flux in boundary layer, L^2/t
$\hat{Q}$	dimensionless excess particle flux
$\hat{Q}_{cr}$	critical excess particle flux for cake formation, dimensionless
Q_v	volumetric flow rate, L^3/t
r	radius, or radial coordinate, L
r_d	drum radius, L
r_i	inside radius, L
r_o	outside radius, or emulsion globule radius, L
r_p	pore radius, L
r_t	tube radius, L
R	gas constant, ML^2/t^2T mol, or rejection of solute, or recycle ratio, dimensionless
R_c	cake resistance, M/L^2t (or pt/L), or L^{-1}
$\hat{R}_c$	specific cake resistance per unit thickness, L^{-2}
R_c'	specific cake resistance (mass basis), L/M
R_e	electrical resistance, V/A
Re	Reynolds number, $dv\rho/\eta$, dimensionless
R_f	reaction rate for extraction per interfacial area, mol/L^2t (or kg-equivalent/m^2s)
R_i	rejection of solute species i, or interception parameter, dimensionless
R_m	membrane resistance, M/L^2t (or pt/L), or L^{-1}
R_{mf}	final membrane resistance, L^{-1}
R_{mi}	initial membrane resistance, L^{-1}
R_r	reaction rate for stripping per interfacial area, mol/L^2t (or kg-equivalent/m^2s)
s	cake compressibility factor, dimensionless
S	entropy, ML^2/t^2T or E/T, or shape factor for flux correction in a cylindrical geometry, dimensionless
S_c	specific surface area (pore surface area/solids volume) in cake, L^{-1}
Sc	Schmidt number, $\eta/\rho D$, dimensionless
Sh	Sherwood number, k_iL/D, dimensionless
S_m	specific surface area (pore surface area/solids volume) in membrane, L^{-1}
t	time, t
$t_{1/2}$	half-life, t
t_i	transport number of ionic species i, dimensionless
T	temperature, T
T_b	normal boiling point, T
T_c	critical temperature, T
T_g	glass transition temperature, T
u_i	absolute mobility of species i, t mol/M or L^2 mol/Et
v	velocity, L/t
v_e	velocity of the external phase, L/t
v_L	inertial lift velocity for constricted tube or channel, L/t
$v_{L,0}$	inertial lift velocity for unconstricted tube or channel, L/t
v_s	superficial face velocity, L/t
V	volume, L^3
V_e	volume of the external phase, L^3
V_f	fractional free volume, dimensionless
V_i	total volume of the internal phase, L^3
V_m	volume of the membrane phase, L^3
V_s	suspension volume, L^3
$\bar{V}_i$	partial molar volume of species i, L^3/mol
w	cake mass per unit membrane area, M/L^2
w_i	mass fraction of species i, dimensionless
w_1	penetrant mass fraction, dimensionless
W	channel width, or drum width, or width of membrane sheet, L
W_e	total consumption amount of the reagent in the external phase, kg-equivalent
We	Weber number, $\omega^2 d_s^3 \rho_e/\gamma$, dimensionless
W_i	total consumption amount of the reagent in the internal phase, kg-equivalent
x_{cr}	critical distance for cake formation, L
x_i	mole fraction of species i, dimensionless
y_i	mole fraction of species i in permeate, dimensionless
z	valence, dimensionless, or z coordinate, L
z_i	valence of species i, dimensionless

Greek Letters

α	selectivity, or mobility ratio ($D_{AB}c_T/D_Ac_{A0}$) for facilitated transport, or

	flow distribution parameter, dimensionless
α_{ij}	separation factor, $(y_i''/y_j'')/(y_i'/y_j')$, y_i = c_i, p_i, w_i, x_i, etc., dimensionless
$\Delta\alpha$	difference in polymer thermal expansion coefficients above and below glass transition, T^{-1} (or $°K^{-1}$)
β	matrix model coefficient in diffusion expression, L^3 polymer/L^3 (STP) [or cm^3 polymer/cm^3 (STP)]
$\Delta\beta$	difference in polymer compressibility above and below glass transition, Lt^2/M or p^{-1} (or atm^{-1})
γ	surface or interfacial tension, M/t^2 or E/L^2, or plasticization parameter in the free-volume model, dimensionless
γ_i	activity coefficient of species i, dimensionless
$\dot{\gamma}$	shear rate, t^{-1}
$\dot{\gamma}_0$	shear rate at edge of boundary layer, t^{-1}
Γ	tubesheet length, L
$\Gamma°$	inlet ratio of the internal reagent equivalents to the feed solute equivalents, dimensionless
Γ_i	ratio of the internal reagent equivalents to the external phase solute equivalents for stage i, dimensionless
δ	polarization layer thickness, or stagnant film thickness, L, or solubility parameter (with subscript), $(E/L^3)^{1/2}$
δ_c	cake thickness, L
ϵ	porosity, or void fraction, or inhomogeneity factor, dimensionless
ϵ_s	suspension porosity, dimensionless
ε	inverse Damköhler number, Da^{-1}, dimensionless
η	viscosity, M/Lt, or efficiency, dimensionless
η_0	pure fluid viscosity, M/Lt
η_d	single fiber efficiency due to diffusion, dimensionless
η_e	viscosity of the external phase, M/Lt
η_i	single fiber efficiency due to interception, dimensionless
η_m	viscosity of the membrane phase, M/Lt
η_s	solvent viscosity, M/Lt, or single collector efficiency, dimensionless
θ	diffusion time lag, or time constant, t, or stage cut, or angle, dimensionless
θ_f	angle subtended by submerged drum, dimensionless
λ	ratio of species diameter to pore diameter, or parameter of the advancing front model, dimensionless
Λ	reduced filter coefficient, dimensionless
μ	chemical potential, ML^2/t^2 mol or $E/$mol
υ	kinematic viscosity, L^2/t
υ_i	number of ions per molecule of electrolyte i
ξ	current utilization, or flow redistribution decrement parameter, dimensionless
π	osmotic pressure, M/Lt^2 or p
ρ	density or mass concentration, M/L^3
ρ_0	pure fluid density, M/L^3
ρ_e	density of the external phase, M/L^3
ρ_m	density of the membrane phase, M/L^3
ρ_s	cake solids density, M/L^3
σ	reflection coefficient, or inhomogeneity factor, dimensionless
σ_c	matrix model coefficient in solubility expression, L^3 polymer/L^3 (STP) [cm^3 polymer/cm^3 (STP)]
σ_0	infinite dilution solubility coefficient in matrix model, L^3 (STP)/(L^3 polymer · M/Lt^2) (or cm^3 (STP)/(cm^3 polymer · atm)]
τ	tortuosity factor, or number of pore volumes of fluid passed through filter, dimensionless
τ_c	cake fouling time constant, t
τ_m	membrane fouling time constant, t
τ_w	wall shear stress for constricted tube or channel, M/Lt^2
τ_{w0}	wall shear stress for unconstricted tube or channel, M/Lt^2
ϕ	volume fraction, or solids volume fraction, dimensionless
ϕ_s	suspension solids volume fraction, dimensionless
ϕ_w	solids volume fraction at cake surface, dimensionless
ψ	electric potential, V
ψ_s	solvent association factor, dimensionless
ω	stirring rate or impeller speed, rpm
Ω	angular velocity, t^{-1}

Diacritical Ma

-	per mol
^	per unit
-	average
.	time rat

Superscripts

'	value ir
	stream s
	of the n
	external
"	value in
	value or
	low-pre
	value in
	sence o
°	standarc
*	ideal ca

Diacritical Marks

˜	per mole
ˆ	per unit mass
¯	average value
˙	time rate of change

Superscripts

′	value in the feed stream, on the upstream side or on the high-pressure side of the membrane, or value in the phase external to the membrane
″	value in permeate, product or extract, or value on the downstream side or on the low-pressure side of the membrane
	value in the membrane indicated by absence of superscript
°	standard reference state
*	ideal case

Subscripts

0	initial value
A, B	particular species
b	bulk
c	cake
f	feed
i	general species index or solute species i
in	inlet
int	interface
j	species j
l	liquid
lm	logarithmic mean
m	membrane
out	outlet
p	product, permeate, permeant, or polymer
r	retentate or reject
s	solution or shell side
t	tube or tube side
T	total
v	vapor
w	water or solvent
x,y,z	three coordinate directions